Entergy

Entergy Operations, Inc.
1340 Echelon Parkway
Jackson, Mississippi 39213-8298
Tel 601-368-5758

F. G. Burford
Acting Director
Nuclear Safety & Licensing

CNRO-2004-00023

April 12, 2004

U. S. Nuclear Regulatory Commission
Attn.: Document Control Desk
Washington, DC 20555-0001

SUBJECT: Request for Alternatives ANO1-R&R-005 and ANO1-R&R-006 - Proposed Alternatives to ASME Weld Repair and Examination Requirements for Repairs Performed on Reactor Vessel Head Penetration Nozzles

Arkansas Nuclear One, Unit 1
Docket No. 50-313
License No. DPR-51

REFERENCES:

1. Entergy Operations, Inc. letter CNRO-2004-00006 to the NRC dated February 23, 2004
2. Entergy Operations, Inc. letter CNRO-2004-00014 to the NRC dated March 4, 2004
3. Entergy Operations, Inc. letter CNRO-2004-00022 to the NRC dated April 8, 2004

Dear Sir or Madam:

In References 1 and 2, Entergy Operations, Inc., (Entergy) submitted Requests for Alternative ANO1-R&R-005 and ANO1-R&R-006 for use at Arkansas Nuclear One, Unit 1 (ANO-1). Specifically, these requests proposed alternatives to the requirements of ASME Sections III and XI as applied to reactor pressure vessel (RPV) head penetration nozzles.

Representatives of the NRC staff and Entergy discussed these requests in a telephone conversation held on March 29, 2004. In that call, the staff asked Entergy to provide written responses to several questions and to also provide a copy of supporting ANO Calculation 86-E-0074-154. (This calculation was provided to Entergy by Framatome-ANP, Inc. as Framatome Document 32-5012424.)

In addition, Entergy informed the staff of the need to revise ANO1-R&R-006 to include a proposed alternative to the requirements of ASME Section XI IWB-3613(b) for evaluating flaws in areas where bolt-up loads play a significant role. Entergy committed to provide to the staff a preliminary analysis report that supports the revised request. (Entergy submitted the revised ANO1-R&R-006 to the staff via Reference 3.)

A047

By this letter, Entergy is providing the following information:

- Responses to the staff's questions pertaining to ANO1-R&R-005 and ANO1-R&R-006 (Enclosure 1)
- The technical report that contains preliminary analysis supporting ANO1-R&R-006 (Enclosure 2), which Entergy committed to provide to the NRC staff in Reference 3
- A copy of ANO Calculation 86-E-0074-154 (Framatome Document 32-5012424) (Enclosure 3)

Framatome-ANP, Inc., the owner of Framatome Document 32-5012424, considers information contained in this document to be proprietary and confidential pursuant to 10 CFR 2.390(a)(4) and 10 CFR 9.17(a)(4). As such, Framatome has requested that it be withheld from public disclosure. The affidavit supporting this request is provided in Enclosure 4. Framatome has also informed Entergy that they consider the vast majority of information contained in the document to be proprietary; therefore, a nonproprietary version was not provided.

If the staff has any questions regarding the proprietary designation of Framatome Document 32-5012424, please contact Mr. James Mallay, Director, Regulatory Affairs for Framatome at the following address and/or telephone number:

Framatome-ANP, Inc.
P. O. Box 10935
3315 Old Forest Road
Lynchberg, VA 24506-0935
Telephone # (434) 832-3000

Submitting the preliminary analysis results fulfills the commitment Entergy made in Reference 3 to provide this information to the staff.

Should you have any questions regarding this letter, please contact Guy Davant at (601) 368-5756.

This letter contains one new commitment as identified in Enclosure 5.

Very truly yours,

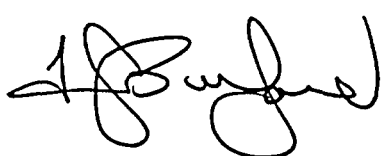

FGB/GHD/ghd

Enclosures:
1. Response to Request for Additional Information
2. Technical Report Supporting ANO1-R&R-006
3. ANO Calculation 86-E-0074-154 (Proprietary Information)
4. Affidavit for Withholding Information from Public Disclosure
5. Licensee-Identified Commitments

cc: (see next page)

cc: Mr. W. A. Eaton (ECH) (w/o Enclosure 3 and 4)
Mr. J. S. Forbes (ANO) (w/o Enclosure 3 and 4)

Dr. Bruce. S. Mallett (w/o Enclosure 3 and 4)
Regional Administrator, Region IV
U. S. Nuclear Regulatory Commission
611 Ryan Plaza Drive, Suite 400
Arlington, TX 76011-8064

NRC Senior Resident Inspector (w/o Enclosure 3 and 4)
Arkansas Nuclear One
P. O. Box 310
London, AR 72847

U. S. Nuclear Regulatory Commission
Attn: Mr. T. W. Alexion (w/all Enclosures)
MS O-7 D1
Washington, DC 20555-0001

ENCLOSURE 1

CNRO-2004-00023

RESPONSE TO NRC REQUEST FOR ADDITION INFORMATION
PERTAINING TO ANO1-R&R-005 & ANO1-R&R-006

ARKANSAS NUCLEAR ONE, UNIT 1

REQUEST FOR ADDITIONAL INFORMATION PERTAINING TO REQUESTS FOR ALTERNATIVES ANO1-R&R-005 & ANO1-R&R-006

By letters dated June 6, 2003, February 23, 2004, and March 4, 2004, Entergy submitted proposed relief requests ANO1-R&R-005 and ANO1-R&R-006 for use at ANO-1. The technical basis for ANO1-R&R-006 is documented in ANO Calculations 86-E-0074-156, -160, -161, and -164, which were submitted on November 26, 2002, to support Request No. ANO1-R&R-004. Non-proprietary versions of Calculations 86-E-0074-156 and -161 were submitted on December 16, 2002. (Calculations 86-E-0074-160 and -164 were submitted as entirely non-proprietary.)

ANO1-R&R-006

By letter dated March 4, 2004, Entergy submitted its technical basis as documented in Engineering Report M-EP-2004-002 to support its decision not to perform water jet conditioning treatment on the repaired region of the CRDM nozzles.

1. Entergy indicated in the cover letter of the March 4, 2004, submittal that it has two concerns regarding ANO Calculation 86-E-0074-156. Entergy has committed to submit a revised fracture mechanics analysis by June 1, 2004. In light of pending revision, Entergy needs to clarify as to the status of ANO Calculation 86-E-0074-156 with respect to the proposed Relief Requests ANO1-R&R-005 and ANO1-R&R-006.

   Response:

   ANO Calculation 86-E-0074-156 was only applicable to Relief Request ANO1-R&R-006. However, because of our discovery, this calculation is being completely superseded by a new calculation as discussed in revised Request for Alternative ANO1-R&R-006, which was submitted to the NRC staff via Entergy letter CNRO-2004-00022 dated April 8, 2004. ANO Calculation 86-E-0074-156 is no longer used as the basis of any requests for ANO-1. As discussed in the responses to questions below, Entergy is providing in Enclosure 2 of this letter a preliminary technical report to support the NRC staff's review of our request. As previously committed, Entergy will submit a final, completed analysis report by June 1, 2004.[1]

[1] Entergy made this commitment in its letter CNRO-2004-00022 to the NRC dated April 8, 2004.

Questions on CNRO-2004-00014, Enclosure 1, dated March 4, 2004

2. Page 4: Describe the flaw model in the revised fracture mechanics calculations:

   a. Describe the location of the initial and final flaw.

   Response:

   The initial flaw is located at both the uphill and downhill locations. The entire J-groove weld prep (J-groove weld and butter) are assumed to be completely cracked. The figure below (obtained from Figure 2 of the technical report from Enclosure 2t) provides the flaw description at the uphill location. The downhill flaw can be described in a similar manner.

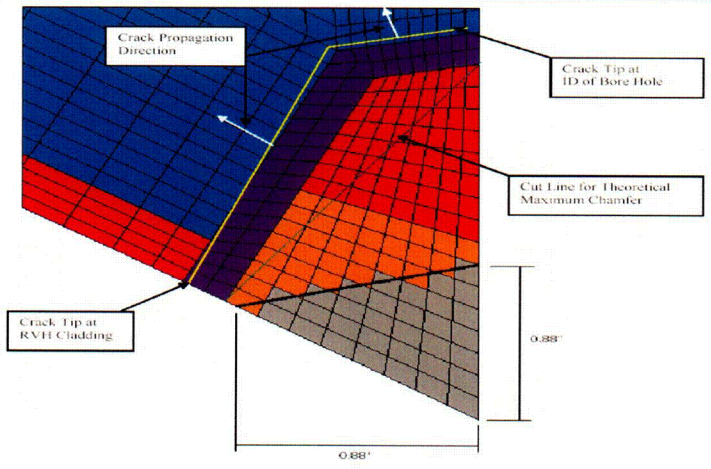

Figure 2: *The flaw geometry with respect to the J-groove weld on the uphill side. The joint configuration is as follows:*

1) *The J-groove weld is the trapezoid shown in red, light brown and grey color.*
2) *The purple color bounding the J-groove weld is the buttering layer.*
3) *The light blue color beyond the buttering layer is the low alloy steel reactor vessel head (RVH).*
4) *The magenta color strip is the stainless steel cladding on the RVH inside diameter (ID) surface.*

The flaw geometry is defined as follows:

1) *The flaw tip (crack front) is along the interface between the buttering layer and the RVH (shown by yellow line)*
2) *Two flaw regions are marked; a) the design maximum chamfer case shown by the colored elements in red, light brown and the buttering in dark blue (note the chamfer size of 0.88 inch), and b) the maximum chamfer line shown in light turquoise color (the crack is the entire J-weld prep.* ***Note:*** *The design minimum chamfer size of 0.63 inch is not shown and would be of a size in-between the "no chamfer" and the design maximum chamfer geometry.*
3) *The "no chamfer" flaw would be composed of the grey, light brown, red, and purple colored elements.*
4) *The crack propagation direction is shown by white arrows.*

The final flaw shape is not shown because the fatigue crack growth analysis showed that the growth estimated for one cycle of operation to be 0.005 inch. The fatigue crack growth analysis is presented in the technical report (Enclosure 2). The small extent of growth would not impact the initial flaw size considered in the analysis.

b. Specify the length and depth of the initial flaw.

Response:

The length and depth of the flaw are the weld prep size for the uphill and downhill locations, which were modeled in the finite element analysis. The finite element models were developed based on design drawings. The weld prep design tolerance was included in the model development. The sketch below shows the weld dimensions and the approximate flaw shapes for the various chamfers considered in the analysis. The two sketches (uphill and downhill) provide the information for the initial flaw sizes considered in the analysis.

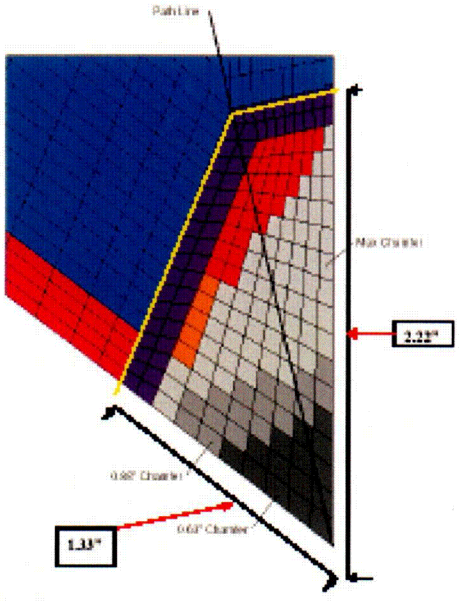

Sketch showing uphill location, chamfer size and initial weld size. The initial flaw sizes for the various chamfer sizes are different. The yellow lines define the crack tip.

Uphill J-Groove Weld

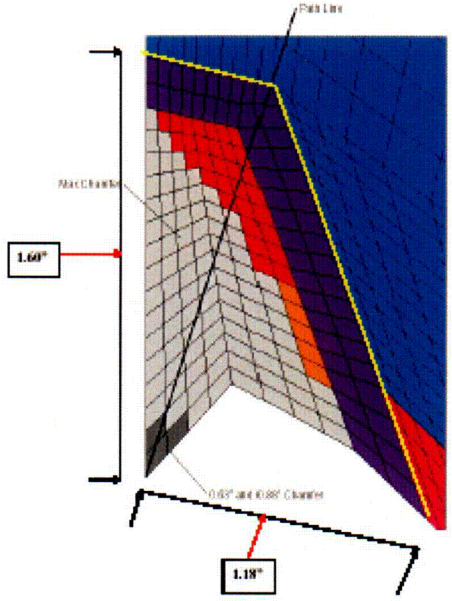

Sketch showing downhill location, chamfer size and initial weld size. The initial flaw sizes for the various chamfer sizes are different. The yellow lines define the crack tip.

Downhill J-Groove Weld

c. Describe the path of crack propagation.

Response:

The flaw propagation direction is marked in the figure above and assumes a self-similar growth for fatigue crack propagation.

C02

d. Clarify whether the final crack is 100% through wall of the J-groove and butter weld.

Response:

Yes, the flaw modeled encompasses the entire J-groove weld prep, which includes the J-groove weld and the butter. The crack front is located at the interface between the butter and the low alloy steel base metal of the RVH.

e. Clarify whether the flaw selected is a worse-case scenario flaw.

Response:

Yes, the flaw size considered is the worst-case scenario since the entire J-groove weld prep is considered cracked. Primary water stress corrosion cracking (PWSCC) is not a plausible cracking mechanism for low alloy steel in the PWR reactor coolant environment. Hence, the assumed flaw is the maximum possible crack that could be caused by PWSCC of the Inconel Alloy 600 weld material.

3. Page 4, fourth paragraph: It is stated that the outmost nozzle penetration will be used in the analysis because it would give the bounding values. Explain this statement in terms of stress distributions.

Response:

Previous industry evaluations (such as those discussed at a 1994 EPRI Workshop on PWSCC of Alloy 600 in PWRs) have shown that the magnitude of the hoop stress due to residual stresses created by welding increases as the nozzle penetration angle with respect to the head (nozzle-to-head angle) increases. In addition, Entergy analysis results for ANO-1, ANO-2, and Waterford Steam Electric Station, Unit 3 (WSES-3) have confirmed this trend. Hence, the hoop stress would be a maximum and would provide an upper bound scenario for the outermost nozzle, which has the highest nozzle-to-head angle.

4. Page 5, first paragraph:

a) Entergy stated that "...Relaxing the residual stresses due to cracking will not be utilized since the analysis will use a linear elastic formulation..." Clarify whether this approach will provide conservative results.

Response:

Relaxation of residual stresses as the crack grows has not been demonstrated by detailed analysis and benchmarked by experimental studies. Studies conducted for girth welds in carbon steel pipes (provided in Attachment 1 of this enclosure) have shown that welding introduces significant constraint, while simultaneously increasing the crack driving force. The analyses and experiments conducted for welded and unwelded pipes showed that the "J-integral" at failure initiation for the ***welded*** *pipe was 63% lower than that for an* ***unwelded*** *pipe. This reduction was attributed to the significant constraint induced by the residual stress field. The experiments were carried out on flawed pipes.*

Had relaxation of the residual stresses occurred during the creation of the flaw, prior to the fracture testing, the drop in the "J-integral" value at initiation for the welded pipe would not have been significantly lower than that for the unwelded pipe. This is further confirmed by testing performed on single-edge notch bend (SE-B) specimens. In this case, the specimen removed from the welded pipe showed a 26% drop in the "J-integral" at fracture initiation. The lower drop caused relaxation during the specimen removal operation. However, the specimen removal did not fully relax the residual stress; otherwise, there would have been an insignificant drop in the "J-integral" value at fracture initiation. The information presented in this study (provided in Attachment 1) indicates that residual stresses do not relax as the crack propagates, because relaxation of residual stresses would manifest as a reduction in the constraint, which was not observed.

Therefore, not considering relaxation of the residual stresses provides a better characterization of the potential for brittle fracture; hence, it can be considered as providing a conservative result. A more accurate description would be "consideration of residual stresses provides a more accurate and representative characterization of the potential for brittle fracture."

b) Entergy also stated that "...The stresses obtained from the residual stress analysis will be entered as crack face pressure. Reactor vessel internal pressure on the crack face will be added to the pressure distribution obtained from the residual stress analysis..." Clarify whether this approach will provide conservative results.

Response:

The results presented in the technical report (Enclosure 2) show that adding the reactor internal pressure as additional pressure on the crack face increases the stress intensity factor (SIF) as shown in the figure below. The analysis presented in the technical report demonstrates that consideration of all loading mechanisms (residual stress, operating stress and internal pressure on the crack face) provides a conservative upper bound SIF.

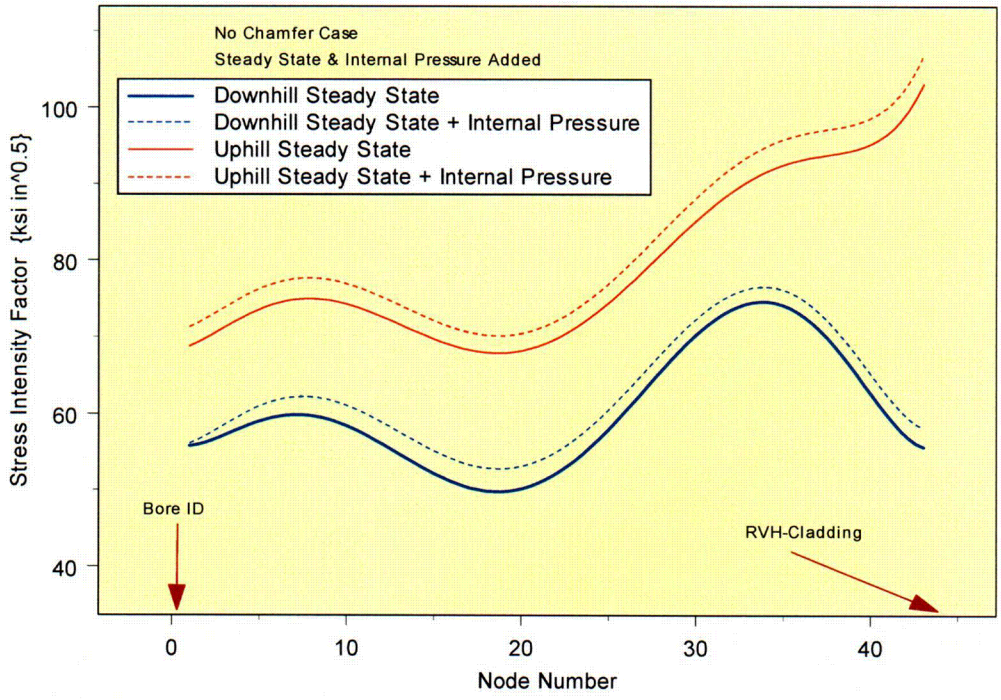

Effect of RCS pressure on "no chamfer" case. The RCS pressure when added to the crack face results in an increase in the SIF. The solid lines are for the total SIF (Residual + Operating + RCS pressure on crack face); the broken lines for the steady state case (Residual + Operating).

c) Describe, step by step, the fracture mechanics analysis.

Response:

The fracture mechanics analysis was performed using the finite element method; no empirical closed form solutions were used. The technical report (Enclosure 2) provides a summary of the fracture mechanics method.

5. Page 5, second paragraph: It is stated that the stress intensity factor will be maximized for use in fatigue evaluation. Describe the fatigue evaluation.

Response:

The fatigue crack growth evaluation is provided as a separate sub-section in the technical report (Enclosure 2).

6. The staff understands that the fracture mechanics analysis will be based on the finite element analysis. Describe whether the results from the revised analysis would be consistent with the calculations performed using either Raju-Newman's solution or Anderson's solution. These two methods are also based on finite element analysis results.

Response:

The Raju-Newman solution commonly used is for part through-wall surface flaws in cylinders. This solution was an empirical correlation developed from several finite element analyses cases. However, the solution was developed for an arbitrary stress distribution, defined by a third order polynomial, through the wall thickness. The Raju-Newman solution is not applicable because:

1) The current flaw geometry (J-groove prep) is a corner flaw in a non-radial bore hole and is not the same as a surface flaw in a cylinder.

2) The stress distribution in the current application is highly non-linear and is very localized. Therefore, a third order polynomial to describe the stress distribution through the wall thickness will not accurately capture the prevailing stress distribution at the interface between the butter and the low alloy steel (where the crack front is located).

Entergy is not aware of an empirical closed form solution developed by Ted Anderson. The solution developed using the J-integral formulation for application in finite element post processing routine has been utilized by others. Entergy has not evaluated this method in detail for application to the current project.

7. Stresses along the crack length vary. It has been shown that stress intensity factors are higher when the stress in the crack center, instead of in the crack tip, is used in the flaw evaluation. Describe how the stresses along the crack length are modeled in the revised analysis.

Response:

The stresses applied in the finite element model used for the current project is applied as a pressure force over the entire crack face. The pressure load is obtained from the stress distribution in the un-cracked stress analysis in the same region. Therefore, the application of the stress, whether at the crack tip or at the center of the crack, is not pertinent to the current analysis.

8. Once the draft fracture mechanics analysis is completed, Entergy needs to submit for staff review the following: preliminary results of the analysis with sufficient explanation, supporting technical basis, and the draft fracture mechanics analysis on docket.

Entergy has included in Enclosure 2 of this letter the preliminary technical report to support revised Request for Alternative ANO1-R&R-006.

Questions on CNRO-2004-00014/Engineering Report M-EP-2004-002 in the March 4, 2004, Submittal

9. Page 15: The staff needs clarification on the postulated flaw model. In Figure 1 of ANO Calculation 86-E-0074-161 in the November 26, 2002, submittal, Entergy assumed a certain flaw size due to lack of fusion to occur at the intersection of the repaired temper bead weld, nozzle, and vessel base metal. Explain why this flaw was not included in the M-EP-2004-002 Calculation in addition to the surface flaw as discussed above.

   Response:

   The flaw considered for the lack of fusion flaw is on the outside diameter (OD) and is not exposed to the reactor coolant. Because of this configuration, this flaw will not be subjected to PWSCC flaw growth; therefore, it was not considered.

10. Page 23: Entergy stated that "...For the initial crack location the stress distribution at the fusion line, the crack tip on the ID surface and the mid-height of the crack are averaged to produce an average stress field that is applied to the crack..." Clarify why the maximum stress field was not applied to the crack.

    Response:

    A similar question was posed by the NRC to Entergy during its review of ANO-2's Relaxation Request #3 pertaining to inspection of RVH incore instrument nozzles. Entergy's response contains an analysis that shows a comparison between the Entergy method for stress averaging and the use of a single maximum stress distribution.[2] The analysis provided showed that the wedge force method produced a SIF that was slightly higher (2.97%) than the moving average method, which was found to be within the expected scatter of 10% for such analysis.

11. Page 23: There is considerable discussion of residual stresses in the flaw evaluation. Discuss whether other applied stresses (e.g., thermal fatigue and pressure) were considered in the stress distribution.

    Response:

    The stresses considered in the fracture mechanics analysis were the operating + residual stress under steady state condition[3]; the reactor internal pressure was added to the membrane stress simulating a crack face pressure.[4] Transient stresses, which would cause fatigue, were not considered since they do not contribute to PWSCC crack growth.

---

[2] See Entergy's response to NRC's Question #2, page 2 of 15 in the Enclosure of Entergy letter CNRO-2003-00048 to the NRC dated September 26, 2003.
[3] See page 9, item 4 of Engineering Report M-EP-2004-002. Entergy submitted M-EP-2004-002 to the NRC via letter CNRO-2004-00014 dated March 4, 2004.
[4] See Engineering Report M-EP-2004-002, Appendix C, Attachment 1, page 6 of 17 and Attachment 2, page 6 of 17.

12. Page 27: Specify the allowable length of an acceptable flaw as presented in Figure 15 on page 27.

    Response:

    The axial flaw length is controlled by a limit load failure; hence, the acceptance limit would be considerably larger than the region of interest. The acceptance limit specified in Table 1, "Reactor Vessel Upper Head Penetration Nozzle Acceptance Criteria," of the NRC's Flaw Evaluation Guidelines and Acceptance Criteria for PWR Reactor Vessel Upper Head Penetration Nozzles[5] *supports this position since this table specifies "no limit" for the axial flaw length.*

13. It seems that Entergy's flaw evaluation did not address flaw growth due to fatigue. Explain.

    Response:

    The period of operation for the current RVH is one cycle of operation. During this period, the design transients that would contribute to fatigue crack growth would be small in number. In addition, experience in evaluating fatigue crack growth using finite element based fracture mechanics analysis and considering operational plus residual stresses (analysis for ANO-2 and WSES-3) have shown that for the design life of forty (40) years the estimated fatigue crack growth is about 0.023 inch. Therefore, the contribution of fatigue crack growth for one cycle of operation is expected to be insignificant. The SIF values at the crack tip were considerably higher than those for the current analysis. The fatigue crack growth in the ANO-2/WSES-3 case would be considerably higher than in the present case. Hence, the use of fatigue crack growth information from the ANO-2/WSES-3 analysis would provide a bounding estimate for the current analysis.

Questions on Appendix D, Evaluation of FTI Repair on a Weld Overlay Repaired Nozzle in the March 4, 2004, Submittal

14. It seems that Entergy has not provided sufficient technical basis to demonstrate the structural adequacy of installing an FTI weld repair on a weld overlay repaired nozzle. Entergy compared only the hoop stresses of an as-built nozzle configuration to the hoop stresses of a J-groove overlay weld configuration. Entergy should have compared the hoop stresses of an FTI weld repair on an overlay repaired nozzle to the hoop stresses of an FTI weld repair on an as-built nozzle. If the hoop stresses are comparable between two models, then Entergy can conclude that the FTI weld repair is acceptable to be installed on an overlay repaired nozzle, assuming other analytical parameters between the two models are comparable. Entergy needs to clarify its technical basis.

[5] The NRC's Flaw Evaluation Guidelines are documented in a letter from Mr. Richard Barrett, NRR, to Mr. Alex Marion, NEI, dated April 11, 2003.

Response:

The purpose of M-EP-2004-002, Appendix D was to compare the prevailing stress distribution at the location where the FTI repair would be instituted. The stresses that contribute to the PWSCC crack growth were found to be predominantly in the hoop direction[6], which would favor axial crack orientation. Therefore, the stress distribution of interest, for the comparison, is the hoop stress. The comparison was performed to demonstrate that the hoop stress distribution at the FTI repair location was unaffected by the installation of an overlay repair on the J-groove weld. Therefore, the analysis in this appendix concluded that the fracture mechanics analysis presented in the body of M-EP-2004-002 would not be affected by the previous J-groove weld overlay; hence, the conclusion that the fracture mechanics analysis presented in the body of the report is valid for those nozzles that were previously repaired with a J-groove weld overlay. The figure below shows a comparison of the prevailing hoop stress for an "as-built condition" and a "weld overlay repair condition". In this figure, the "weld overlay condition" stress contours were superimposed on the "as-built condition" contours. The two black lines represent the region of the weld that attaches the nozzle to the RVH. The nozzle tube fusion line is at the top black line. The axial crack, lower tip, is located at the top black line. Therefore, the region for comparing the prevailing stress distribution is this location. From this figure, it is observed that there is no influence of the "weld overlay" on the hoop stress distribution at this location. Therefore, installing the FTI repair will produce a residual stress distribution at this location would be similar to that for an "as-built condition" requiring the FTI repair.

[6] See page 13 of M-EP-2004-002.

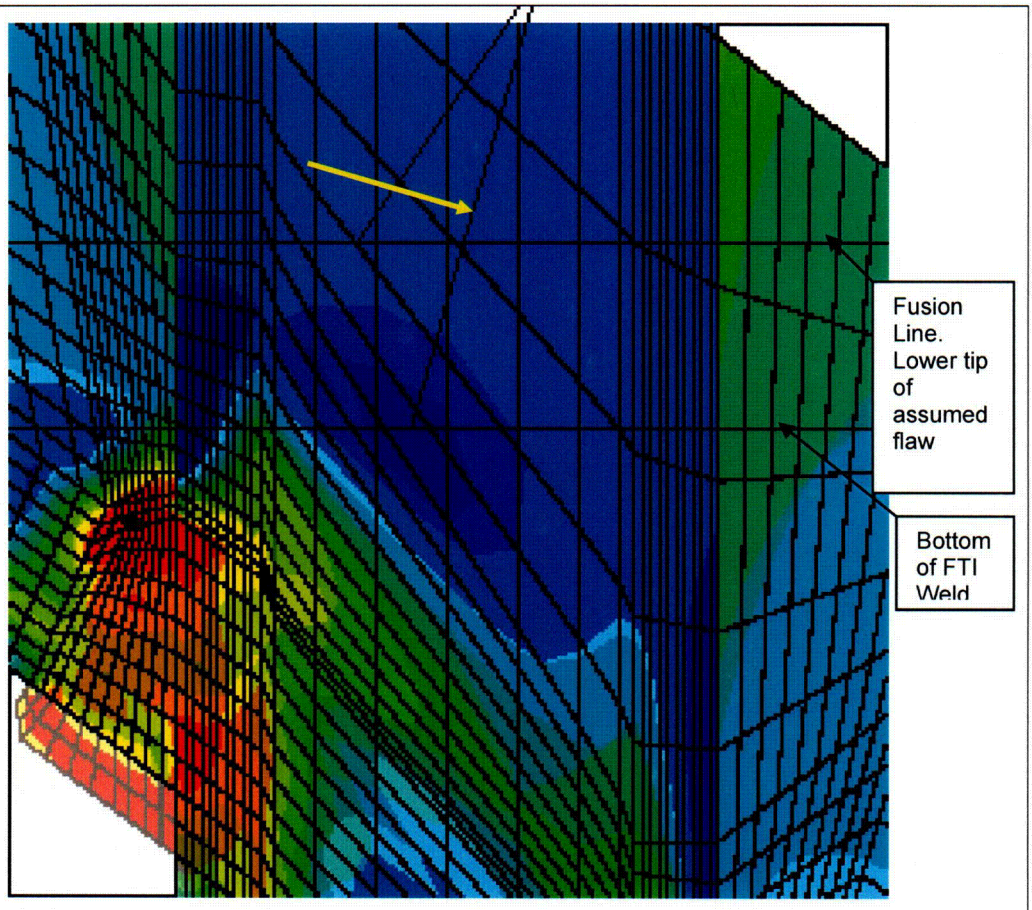

The "weld overlay condition" is superimposed on the "as-built condition" for hoop stress. The region of interest is at the fusion line (upper black line) and is indicated by the yellow arrow. In this region, the coloration of the stress contours is uniform (i.e. no bleed-through effect). This is indicative of very similar stress distributions at this location.

Questions on ANO Calculation 86-E-0074-161 in the November 26, 2002, Submittal

15. Page 23: It is stated that the postulated flaw in the temper bead weld repair was evaluated using residual stresses and fatigue stresses. Discuss whether other stresses such as thermal and pressure stresses were also applied in the flaw evaluation.

Response:

The stresses for the operating conditions (steady state and transient conditions) were obtained from detailed finite element analysis of the RVH geometry. The analysis used the design loading conditions of pressure and temperature for both the steady state and transient analysis. The residual stress analysis was also performed by finite element method, which simulated the important fabrication steps (buttering, post-weld heat treatment, vessel hydrostatic testing, and steady state operation). The resulting stresses

C04

included the thermal and pressure stresses appropriately; therefore, the flaw evaluation considered these stresses.

ANO1-R&R-005

Questions on CNRO-2004-00006/February 23, 2004, Resubmittal of ANO1-R&R-005

16. Page 7: Entergy indicated in its letter dated February 23, 2004, that its repair method leaves a strip of low alloy steel exposed to the primary coolant and that the general corrosion of the low alloy base material is insignificant and is estimated to be 0.0032 inch/year. Entergy also indicates that repair of all 69 RPV head nozzles would present a 16.9% increase in annual release of Fe into the reactor coolant system. Based on the six repaired nozzles from the last outage, has the licensee seen an increase in the release of Fe into the reactor coolant system and if so, is the increase commensurate with the number of nozzles that were repaired based on calculations of general corrosion?

Response:

The parameter measured that would give an indication of a problem from exposed carbon steel in the RCS is Total Suspended Solids (TSS). The plot below is from the first month after startup from refueling outage 1R16 (2001) to present. The two points in the middle show crud results on shutdown and startup for 1R17 (2002). There are no changes in suspended solids; hence, there is no significant change of iron content in the reactor coolant.

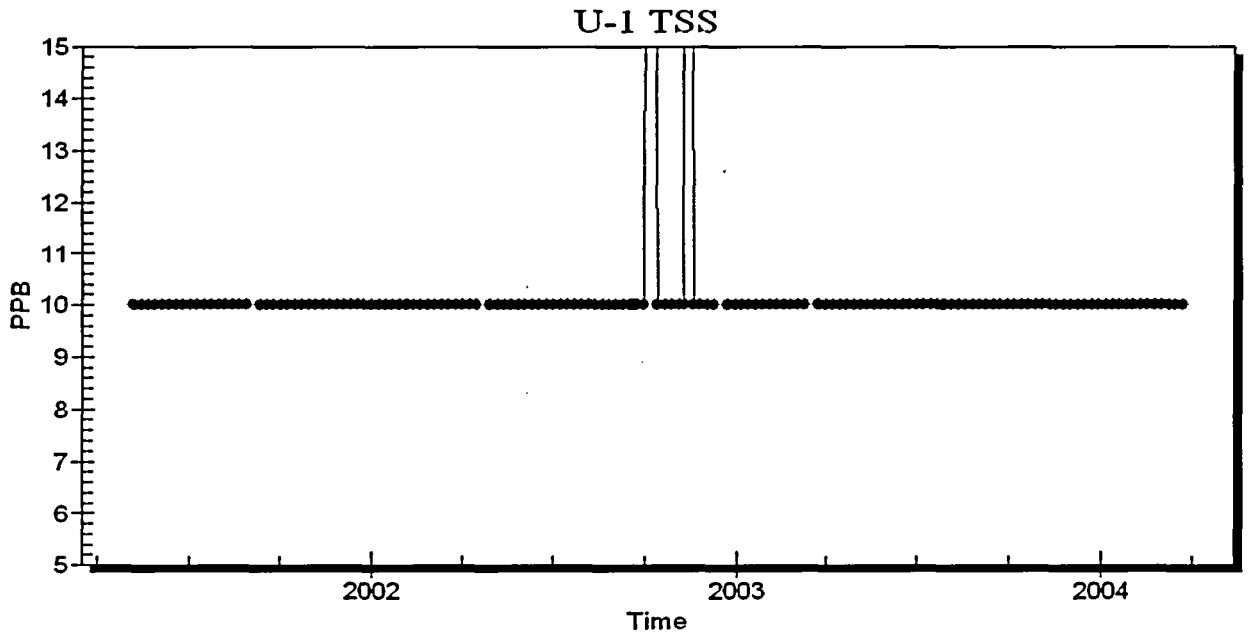

17. Page 7: Entergy discusses an ANSYS analysis performed by Framatome-ANP and calculated stresses that were then compared to ASME Code, Section III, NB-3000 criteria. Please provide analysis and calculations or provide a reference if material has been submitted previously.

Response:

The requested information is contained in ANO Calculation 86-E-0074-154, which is included in Enclosure 3 of this letter.

ANO1-R&R-005 AND R&R-006

18. Entergy needs to provide for staff review inspection results of the six repaired CRDM nozzles as soon as the results are available.

Response:

Entergy will provide periodic status information regarding RPV head penetration inspection results throughout the 1R18 inspection period. This may be accomplished via e-mail, telephone conversations, fax, or other means.

ENCLOSURE 2

CNRO-2004-00023

TECHNICAL REPORT SUPPORTING
REQUEST FOR ALTERNATIVE ANO1-R&R-006

ATTACHMENT 1

TECHNICAL REPORT SUPPORTING REQUEST FOR ALTERNATIVE ANO1-R&R-006

FRACTURE ASSESSMENTS OF WELDED STRUCTURES

Technical Report to Support Relief Request ANO1-R&R-006

Introduction

The review of the fracture mechanics analysis for the J-groove weld remnant, documented in [1], indicates that the analysis was not sufficiently rigorous. Two concerns were identified, which led to the conclusion that the analysis (presented in Reference 1) was not an accurate representation of the prevailing conditions of the J-groove weld remnant. These concerns were:

Concern 1: The stress intensity factor (SIF) equation, used in the analysis of the J-groove weld flaw, in Reference 1 was obtained from Reference 2. The formulation, Figure 1, was a combination of two influence function solutions. The two solutions used to derive a solution [2] for the corner flaw in a nozzle were:

a) A semi-circular crack on a half-space (upper left in Figure 1); and,
b) A quarter-circular crack in a quarter-space (upper right in Figure 1).

The derivation for the corner crack for a nozzle consisted of averaging the coefficients from the two equations for the two other crack models described above. The coefficients for the nozzle corner flaw are shown in the lower right sketch of Figure 1. The averaging of the two coefficients for the linear term (A_1) appears to be in error. The average of the coefficients from the two base models results in a value of 0.511 for the resulting coefficient, whereas the value in the equation is 0.537.

The publication, cited in Reference 2, was published at the request of the ASME Nuclear Codes and Standards Department to provide the information to utility members. The foreword to this publication clearly states that; "*The solutions provided herein are for information only*". Furthermore, the reference cited for this formulation is a personal communication between two individuals. There is no cited reference that provides an analytical basis for the formulation.

The equation, though published in the Electric Power Research Institute (EPRI) document, does not have the necessary confirming documentation to evaluate the validity of its application. Furthermore, the crack geometry, which has a quarter-circular shape, does not define the J-groove weld geometry properly. The J-groove weld geometry is a distorted quarter-ellipse.

Thus, Entergy believes the use of this model is improper because:

a) There is no documented validation of the model; and,
b) The geometry does not adequately represent a J-groove weld.

Concern 2: In the analysis presented in Reference 1 the residual stress distribution from the J-groove welding process was not explicitly considered as an applied stress. Instead, the residual stress profile (for an un-cracked J-groove weld) was used to define the initial flaw size. The justification provided in Reference 1 states in part:

"Although at shutdown, the residual hoop stress in the weld region is high, above 60,000 psi (Figures 5 and 8), the stresses decrease to zero just beyond the butter region and is compressive in the head. These residual stresses would be relieved as the crack propagates through the weld and butter and a short distance into the head. Deeper

Technical Report to Support Relief Request ANO1-R&R-006

cracks would then experience only the compressive residual stress ahead of the crack tip. It can be seen from Figure 8 and Table 4 that the residual stresses are compressive at some distance less than 0.436" into the head. The depth of the initial flaw size will therefore be increased by this amount so that residual stresses need not be considered in the present flaw evaluation".

The evaluation, which used an influence function (weight function) method, is predicated on the following bases [3]:

a) The integration to obtain the weight function is carried out over the depth of the crack "a", and the stress distribution $\sigma(x)$ across the plane of the crack in the uncracked body.
b) The stress distribution when integrated over the depth of the crack is the "force system" with which the stress intensity factor is associated.
c) The "force system" and, therefore, the stress distribution can be arbitrary across the plane of the crack.
d) Only the stress distribution that is bounded by the cracked region is considered in the analysis. The stress distribution ahead of the crack front is of no consequence.

Contrary to the basis of the analytical method (influence function/weight function) that required the stress distribution in the cracked region be considered, the justification provided in Reference 1, and cited above, ignores the contribution from residual stress distribution. Therefore, the assumption made in Reference 1 violates the basis of the method.

Thus, Entergy believes that ignoring the residual stress distribution is improper because:

a) It violates the basis of the method of analysis; and,
b) The results would be non-conservative since the crack face is not loaded by the force from residual stresses in the cracked region.

Technical Report to Support Relief Request ANO1-R&R-006

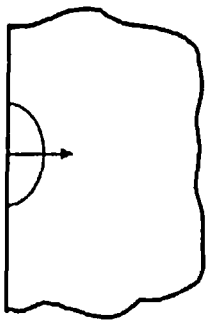

$$K_I = \sqrt{\pi a}\,[.688A_0 + .522(\tfrac{2a}{\pi})A_1 + .434(\tfrac{a^2}{2})A_2 + .377(\tfrac{4a^3}{3\pi})A_3]$$

Semicircular Crack in Half-Space

"a"

$$K_I = \sqrt{\pi a}\,[.725A_0 + .501(\tfrac{2a}{\pi})A_1 + .462(\tfrac{a^2}{2})A_2 + .409(\tfrac{4a^3}{3\pi})A_3]$$

Quarter-Circular Crack in Quarter-Space

"b"

Figure 1: *{Source: Reference 2, page G-21}. Formulation of Nozzle corner crack by the combining of two solutions ("a" and "b") to produce the solution for a nozzle corner crack "c". The coefficient for each term is averaged to yield the corresponding coefficient for the nozzle corner crack. Note the error in the coefficient for the linear (A_1) term. [(0.522+0.501)/2 = 0.5115]*

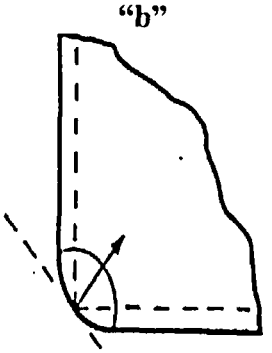

$$K_I = \sqrt{\pi a}\,[.706A_0 + .537(\tfrac{2a}{\pi})A_1 + .448(\tfrac{a^2}{3\pi})A_2 + .393(\tfrac{4a^3}{3\pi})A_3]$$

Simulated Three-Dimensional Nozzle Corner Crack

"c"

In order to resolve the concern in a succinct manner, detailed finite element analyses for the residual stresses and fracture mechanics were undertaken. These analyses were designed to ensure that both the geometry and the loading conditions were accurately represented.

The flaw geometry with respect to the uphill J-groove weld is presented in Figure 2.

Technical Report to Support Relief Request ANO1-R&R-006

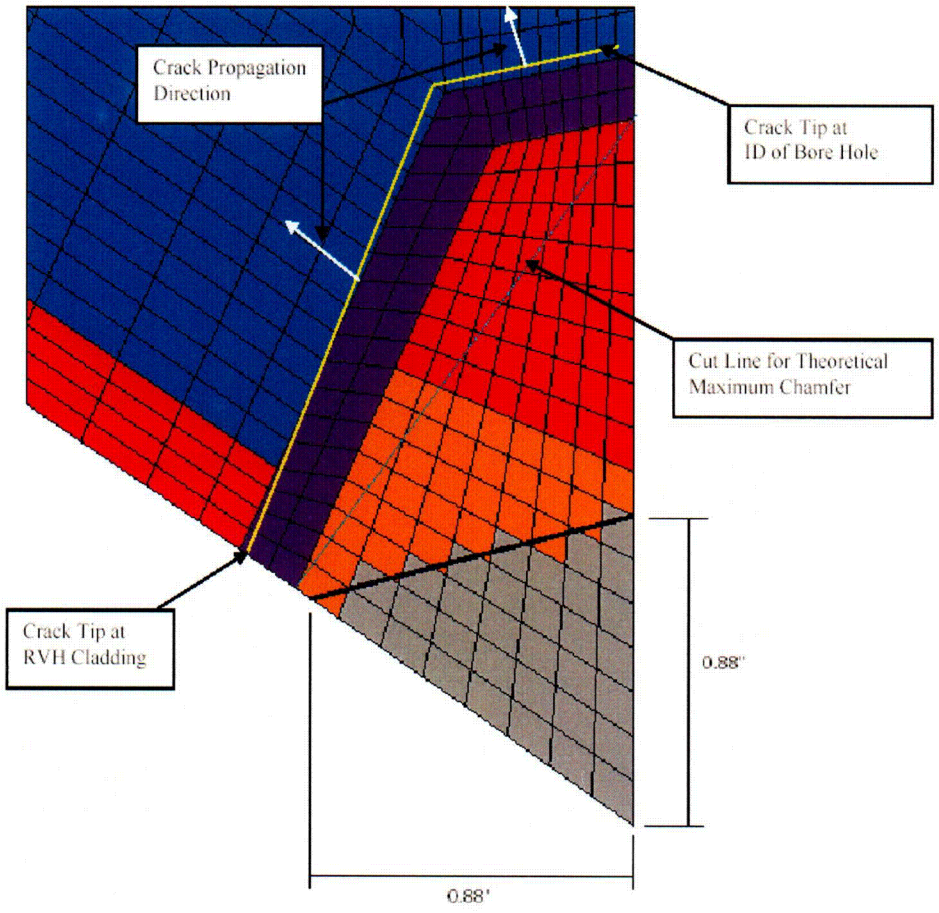

Figure 2: *The crack flaw geometry with respect to the J-groove weld on the uphill side. The joint configuration is as follows:*

1) *The J-groove weld is the trapezoid shown in red, light brown and grey color.*
2) *The purple color bounding the J-groove weld is the buttering layer.*
3) *The light blue color beyond the buttering layer is the low alloy steel reactor vessel head (RVH).*
4) *The magenta color strip is the stainless steel cladding on the reactor vessel head (RVH) inside diameter (ID) surface.*

The flaw geometry is defined as follows:

1) *The flaw tip (crack front) is along the interface between the buttering layer and the RVH (shown by yellow line)*
2) *Two flaw regions are marked; a) the design maximum chamfer case, shown by the colored elements in red, light brown and the buttering in purple (note the chamfer size of 0.88 inch), and b) the maximum chamfer line shown in light turquoise color (the crack is the entire J-weld prep. Note, the design minimum chamfer size of 0.63 inch is not shown and would be of a size in-between the no chamfer and the design maximum chamfer geometry.*
3) *The no chamfer flaw would be composed of the grey, light brown, red and the purple colored elements.*
4) *The crack propagation direction is shown by white arrows.*

C05

Technical Report to Support Relief Request ANO1-R&R-006

The installation of the Framatome Technologies incorporated (FTI) repair design requires the counterboring of the existing nozzle followed by welding the cut nozzle to the reactor vessel head (RVH). The final step in this repair process is the machining of the corner of the remnant J-groove weld to create a chamfer. Since the J-groove weld cannot be inspected by available (qualified) non-destructive examination methods, the weld has to be assumed to be completely cracked (J-groove weld and butter). The J-groove weld butter has an interface with the low alloy steel RVH hence, the assumed flaw has to be evaluated to ascertain the propensity for brittle fracture of the low alloy steel RVH.

Figure 2 is a sketch of the joint geometry at the uphill location. The J-groove weld prep is approximated by two lines that intersect at the knee of the weld prep. In actual practice the J-groove contour is a smooth curve. This approximation is made to simplify the modeling effort and is not expected to significantly impact the results. It is important to note that the theoretical maximum chamfer case is an assumed maximum for the purpose of this analysis. This theoretical maximum chamfer case was included to evaluate the SIF behavior with respect to the chamfer size. Thus, evaluating a full complement, using the "no chamfer" and the "theoretical maximum chamfer" to bracket the two design chamfer sizes, would provide sufficient information for a rational evaluation. Figure 2 shows the finite element mesh that was used in the stress analysis. It should be noted that the finite element mesh used in the fracture mechanics analysis is more refined in the crack region. In this figure the crack front along the buttering layer and the low alloy steel RVH is shown by the yellow line. The crack propagation direction shown assumes a self-similar crack profile and hence, the propagation direction is shown as being orthogonal to the crack front. The crack region for the three chamfer designs is also shown. The bore ID is to the right of the sketch. This figure shows that the assumed crack encompasses the entire J-groove weld including the buttering layer. Since both the J-groove weld and the buttering layer material are made from Inconel Alloy 82/182 (similar to Inconel Alloy 600) it is considered susceptible to primary water stress corrosion cracking (PWSCC). Therefore, the entire weld is assumed to be cracked by a PWSCC mechanism. The low alloy steel RVH material is very resistant to PWSCC under the electrochemical conditions prevailing in the reactor coolant system and is not assumed to be cracked by the PWSCC mechanism. Crack growth into the low alloy steel RVH material would be by a fatigue mechanism.

In the following sections a brief description of the models, the analysis method, results from the analysis and a discussion on the application of an adequate safety factor to ensure against non-ductile failure are presented.

Technical Report to Support Relief Request ANO1-R&R-006

Residual Stress Analysis

As-Built Analysis

The detailed finite element analysis for residual stress determination [4] showed that the hoop and axial stresses tend to increase with the increased penetration angle of the nozzle axis with respect to the RVH. This was found to be the case for the uphill side of the J-groove weld where the nozzle stresses were the highest. In order to develop a bounding analysis, the outermost penetration angle (38.5°) was selected. Since the analyses in Reference 4 also shows that the residual stresses increase with nozzle material yield strength, the analysis was performed with the highest yield strength. In this manner, an upper bound residual stress distribution is obtained. The modeling for determining the residual stresses in the as-built condition [5] was as follows:

1) The finite element mesh consisted of 3-dimensional solid (brick) elements. Four elements were used to model the tube wall with similar refinement carried to the attaching J-weld.

2) The control rod drive mechanism (CRDM) tube material was modeled with a monotonic stress-strain curve. The highest yield strength from the nozzle material bounded by the nozzle group was used. This yield strength was referenced to the room temperature yield strength of the stress-strain curve described in Reference 5. The temperature dependent stress-strain curves were obtained by indexing the temperature dependent drop of yield strength.

3) The weld material was modeled as elastic-perfectly plastic for the weld simulation. This approximation is considered reasonable since most of the plastic strain in the weld metal occurs at high temperatures where metals do not work-harden significantly [6]. The temperature in the weld is high during the welding process. Once the weld begins to cool, the temperatures in the weld at which strain hardening would persist are of limited duration [6]. This was borne out by the comparison between the analysis based residual stress distribution and that obtained from experiments [7].

4) A simulation of the post weld heat treatment (PWHT) was performed after the buttering layer was applied by welding.

5) The J-groove weld is simulated by two passes based on studies presented in Reference 5.

6) After completing the j-groove weld, a simulated hydro-test load step is applied to the model. The hydro-test step followed the fabrication practice.

7) The model is then subjected to a normal operating schedule of normal heat up to steady state conditions at operating pressure. Upon

Technical Report to Support Relief Request ANO1-R&R-006

reaching steady state conditions the normal cooldown cycle is simulated to achieve ambient conditions. At this time the repair models are executed.

The stress contours for the outermost nozzle obtained from the finite element analysis are presented in Figure 3. The stress contour color scheme is as follows:

Dark Navy blue	*from Minimum (Compression) to -10 ksi*
Royal blue	*from -10 to 0 ksi*
Light blue	*from 0 to 10 ksi*
Light green	*from 10 to 20 ksi*
Green	*from 20 to 30 ksi*
Yellow green	*from 30 to 40 ksi*
Yellow	*from 40 to 50 ksi*
Red	*from 50 to 100 ksi*

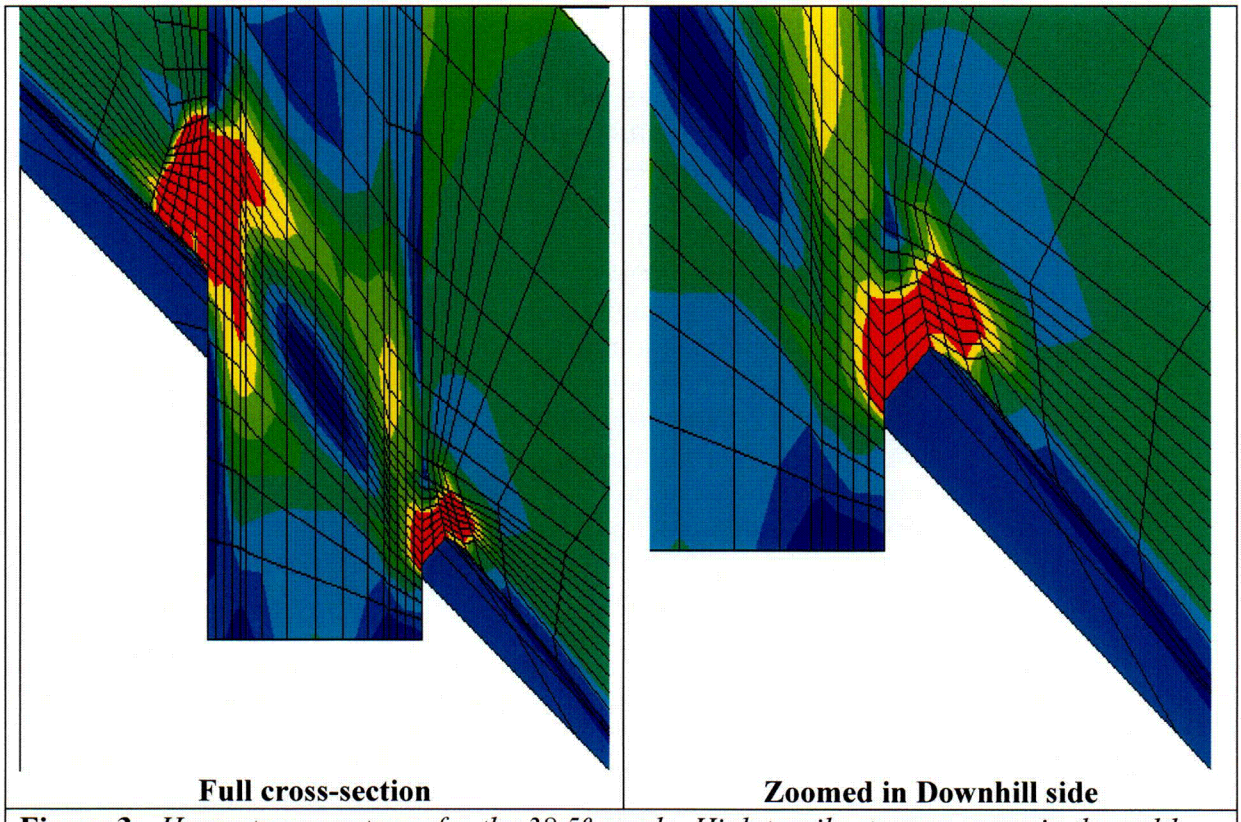

Figure 3: *Hoop stress contours for the 38.5° nozzle. High tensile stresses occur in the weld and adjacent tube material.*

C06

Technical Report to Support Relief Request ANO1-R&R-006

Chamfer Repair Analysis

The repair of the degraded nozzle was accomplished by counterboring the existing nozzle to an elevation that was approximately two (2.0) inches above the top of the uphill weld. The remaining nozzle was secured by roller expansion, which was followed by welding the nozzle end to the RVH by a temper bead welding process. The final repair process involved installing a chamfer on the J-groove weld remnant. This chamfer was made to reduce the J-groove weld size since the fracture mechanics analysis postulates that the entire J-groove weld (including the butter) is cracked. The removal of a portion of the J-groove weld is expected to reduce the flaw size sufficiently such that the stress intensity factor (SIF), based on the reduced flaw size and anticipated loading, is below the allowable limit specified in ASME Code Section XI paragraph IWB-3613(b) [8].

The chamfer design considered in the analysis was based on the design chamfer sizes [9] for the outer most penetration. Two additional cases, a no chamfer and a maximum theoretical chamfer, were evaluated to provide a complete set such that a better correlation between the SIF as a function of chamfer size could be developed. Therefore, the analysis was performed for four J-groove weld remnants, as follows (see Figure 2):

1) No chamfer, J-groove weld left as-is after counterboring.
2) Design minimum chamfer of 0.63 inch. This is the side of an equilateral right angle triangle at the corner of the remnant J-groove weld and is located on the uphill side. The contour is followed to the downhill side as specified in Reference 9.
3) Design maximum chamfer of 0.88 inch. This is the side of an equilateral right angle triangle at the corner of the remnant J-groove weld and is located on the uphill side. The contour is followed to the downhill side as specified in Reference 9.
4) A theoretical maximum chamfer based on a diagonal connecting the bottom of the buttering weld from the RVH bore to the inside of the buttering on the RVH cladding at both the uphill and downhill locations. The chamfer was swept from the uphill to the downhill to obtain the chamfer at intermediate locations in the finite element model.

The residual stresses data for the as-chamfered condition was saved. The model was then subjected to a normal heat-up and steady state sequence. Transient analysis was performed for the following transients:

1) Normal heat-up and cooldown.
2) Reactor trip at full power (normal and upset condition).
3) Inadvertent rod withdrawal (Accident condition).

Technical Report to Support Relief Request ANO1-R&R-006

The stress contours for the residual stresses only and the steady state operating condition (residual + operating stresses) for the various repair cases evaluated are presented in Figures 4 through 7. In these figures, the left contour is for the "residual stress only" case and the right contour is from a case obtained from the steady state operating condition. The steady state operating condition is composed of the prevailing residual stress at the operating temperature and the stresses in the RVH due to pressure and temperature at steady state operating conditions. Hence, steady state operating conditions represent the prevailing stress state at the joint, which results from the combination of the component stress distributions.

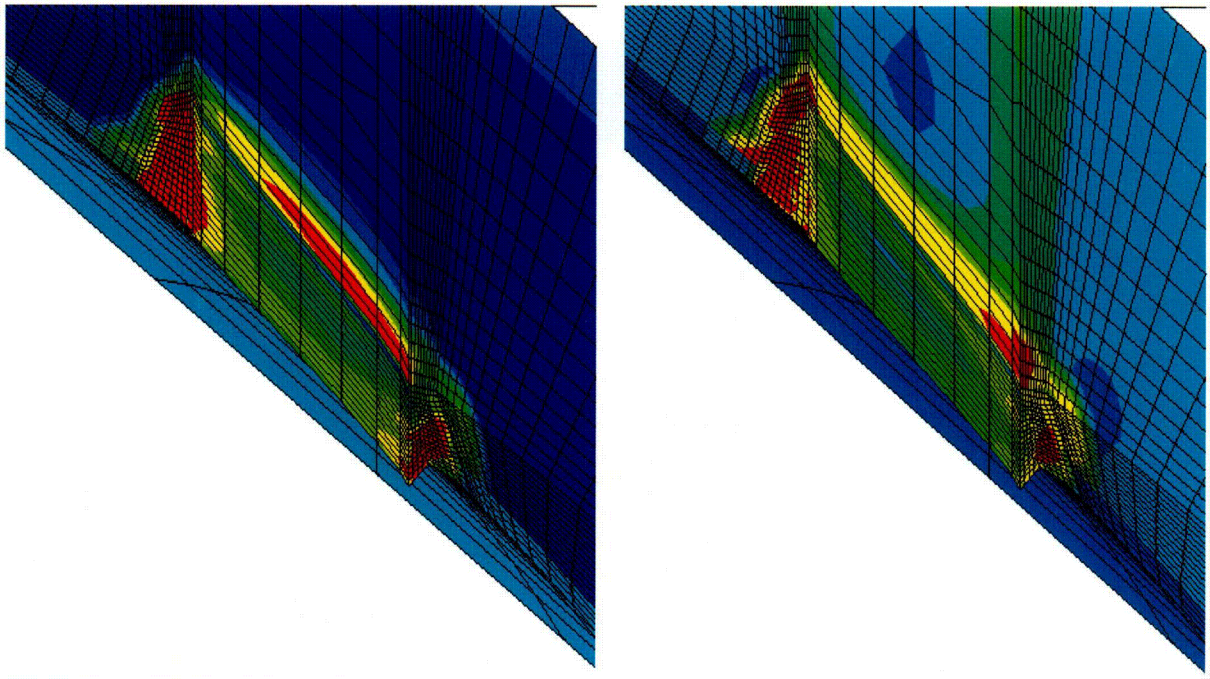

Residual Stresses Only **Residual + Operating (Steady State)**

Figure 4: *Stress contours for the "no chamfer case". The zone of high residual stresses (red color) is observed to shrink in the steady state condition.*

Technical Report to Support Relief Request ANO1-R&R-006

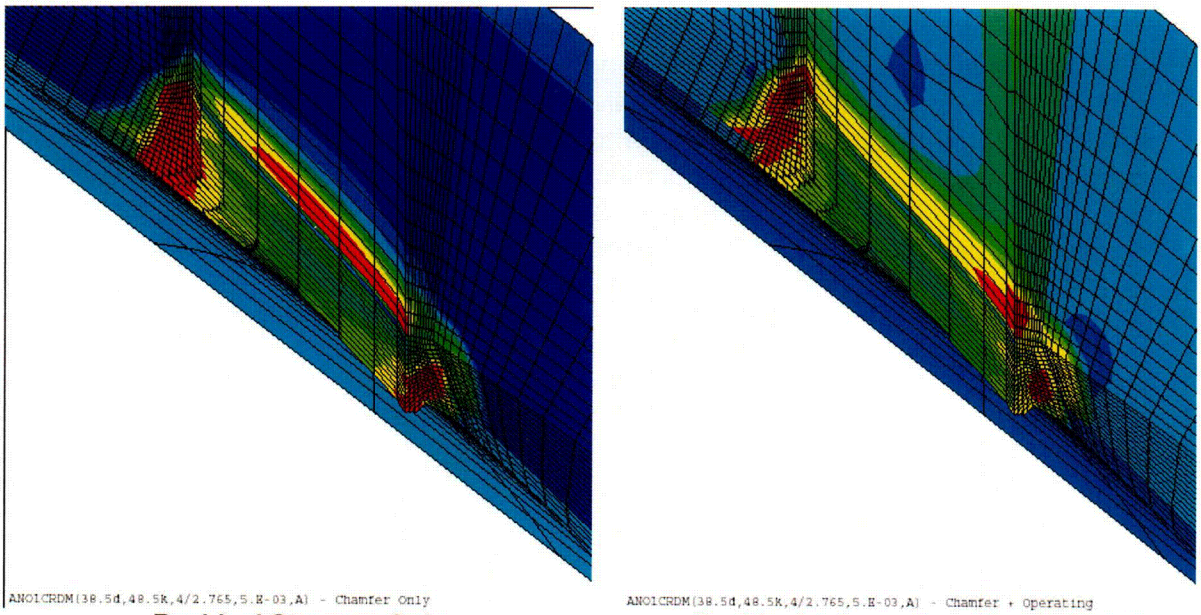

Residual Stresses Only **Residual + Operating (Steady State)**

Figure 5: *Stress contours for the "design minimum chamfer" case. The zone of high residual stresses (red color) is observed to shrink in the steady state condition.*

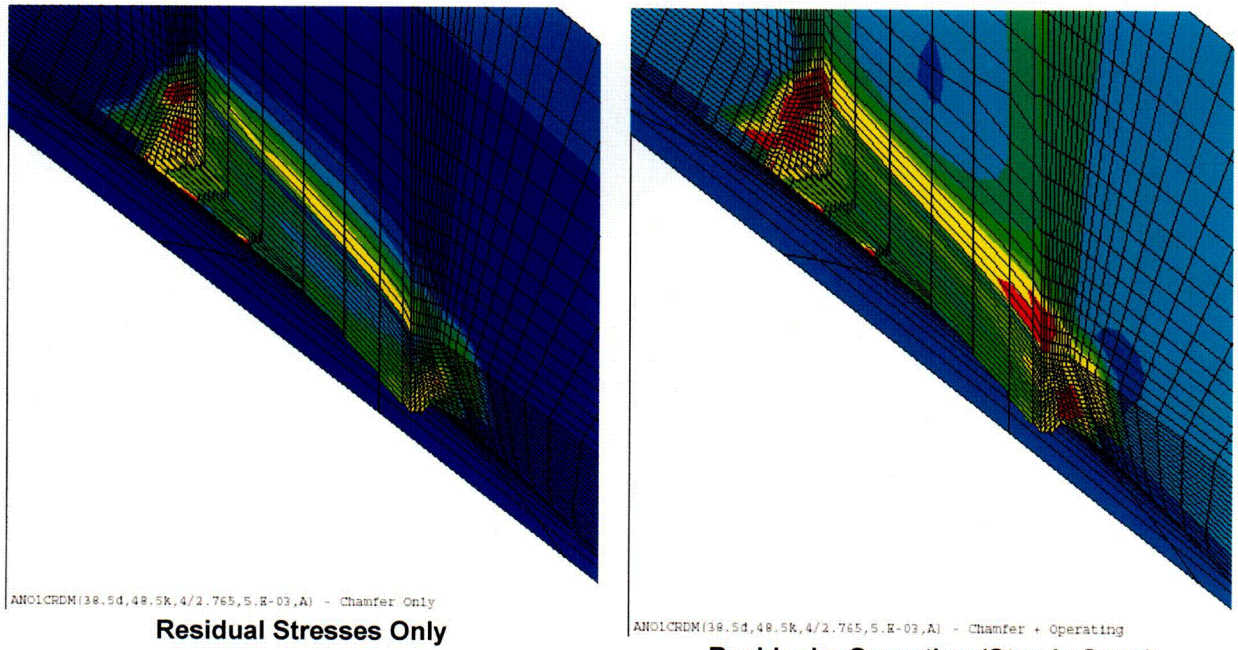

Residual Stresses Only **Residual + Operating (Steady State)**

Figure 6: *Stress contours for the design "maximum chamfer" case. The zone of high residual stresses (red color) is observed to shrink in the steady state condition.*

C08

Technical Report to Support Relief Request ANO1-R&R-006

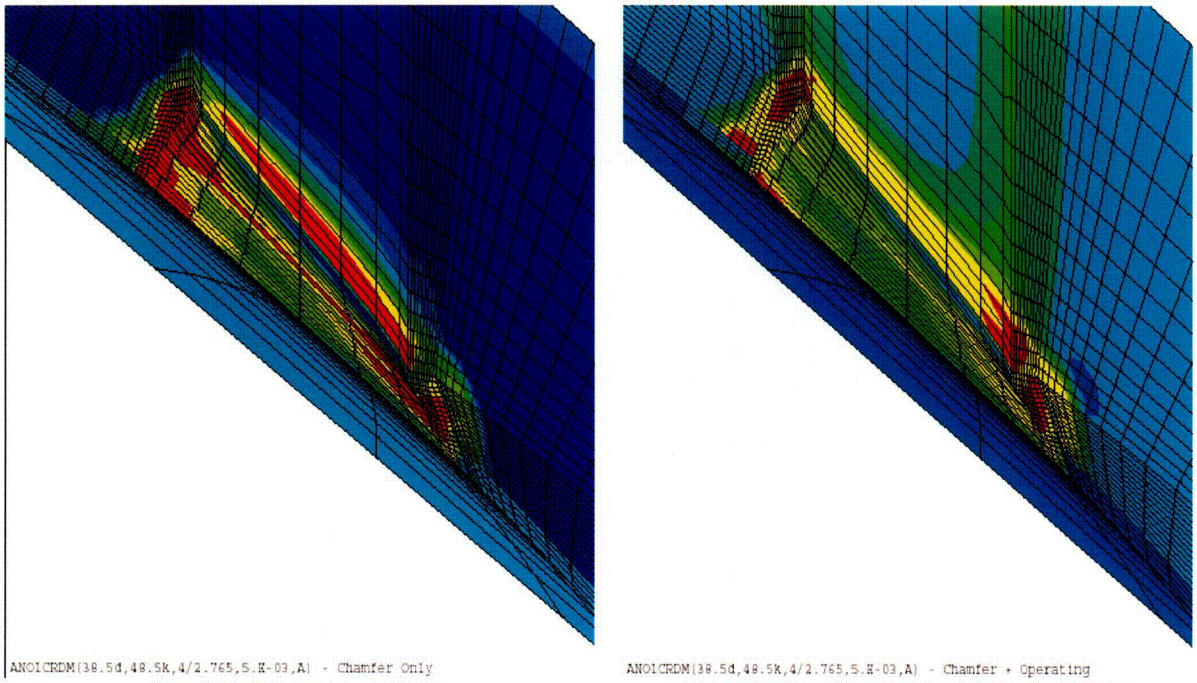

Residual Stresses Only **Residual + Operating (Steady State)**

Figure 7: *Stress contours for the "theoretical maximum chamfer" case. The zone of high residual stresses (red color) is observed to shrink in the steady state condition.*

The hoop stress data obtained from the analysis for the various chamfer designs were evaluated along a path, which originates at the lower corner of the interface between the J-groove weld and the nozzle and extends towards the RVH outside diameter (OD) through the intersection point where the butter interface changes slope. This path is shown in Figure 8 for the downhill location and in Figure 9 for the uphill location. Also shown in these figures are the locations for the different chamfers considered in this analysis.

C09

Technical Report to Support Relief Request ANO1-R&R-006

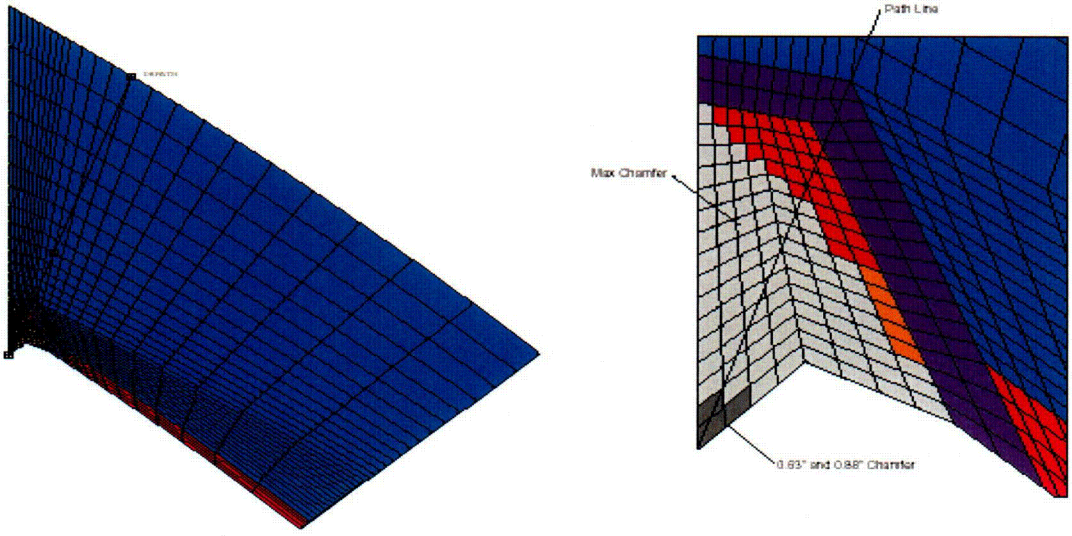

a) Path shown for full RVH **b) Path shown at J-groove weld**

Figure 8: *Path selected for hoop stress evaluation at the downhill location. The proposed chamfer designs and the path direction at the butter-RVH interface are shown in "b" (detail at J-groove weld).*

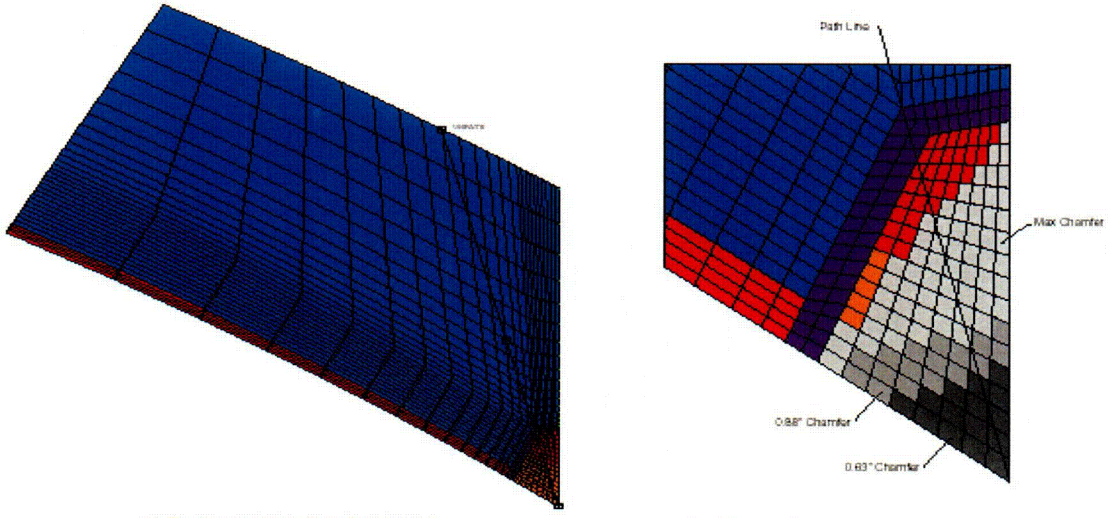

a) Path shown for full RVH **b) Path shown at J-groove weld**

Figure 9: *Path selected for hoop stress evaluation at the uphill location. The proposed chamfer designs and the path direction at the butter-RVH interface are shown in "b" (detail at J-groove weld).*

The hoop stress for the steady state and the "residual stress only" condition were extracted from the output files at about fifty locations. The hoop stress distribution along this path for the various chamfer designs are presented in Figures 10 and 11.

Technical Report to Support Relief Request ANO1-R&R-006

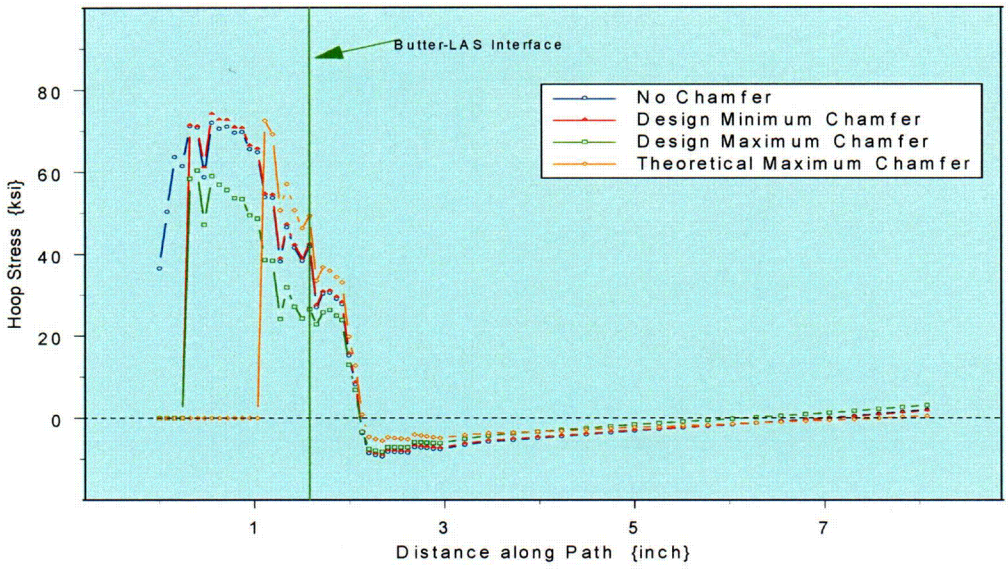

a) Residual Stress Only

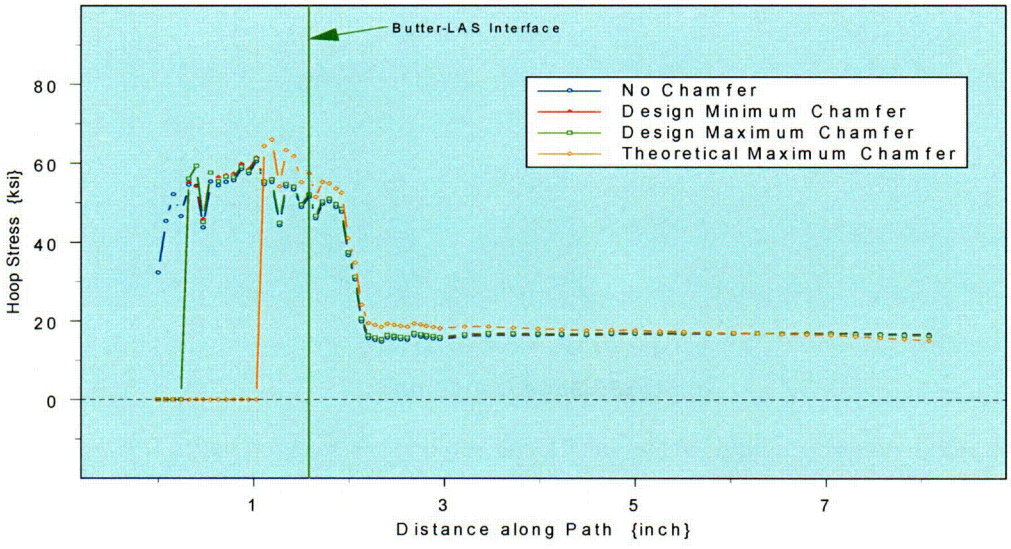

c) Steady State Condition

Figure 10: *Hoop stress distribution at the downhill location along the selected path. The J-groove weld corner is at the left (0.0) and the RVH OD at the right (8.08"). The hoop stress is highly localized to the J-groove weld region. The effect of steady state operation is to soften the peak residual stress in the J-groove weld and eliminates the compression region immediately beyond the interface between the butter and the RVH. The effect of the chamfer design on the peak magnitude appears to be minimal. The location of the butter to RVH interface is shown by the green vertical line, which is located at 1.58 inches from the corner.*

Technical Report to Support Relief Request ANO1-R&R-006

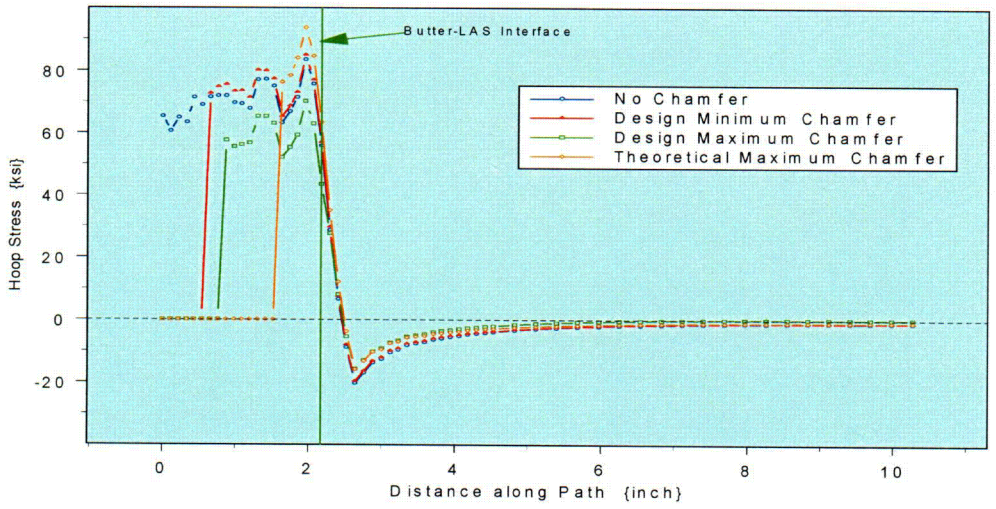

a) Residual Stress Only

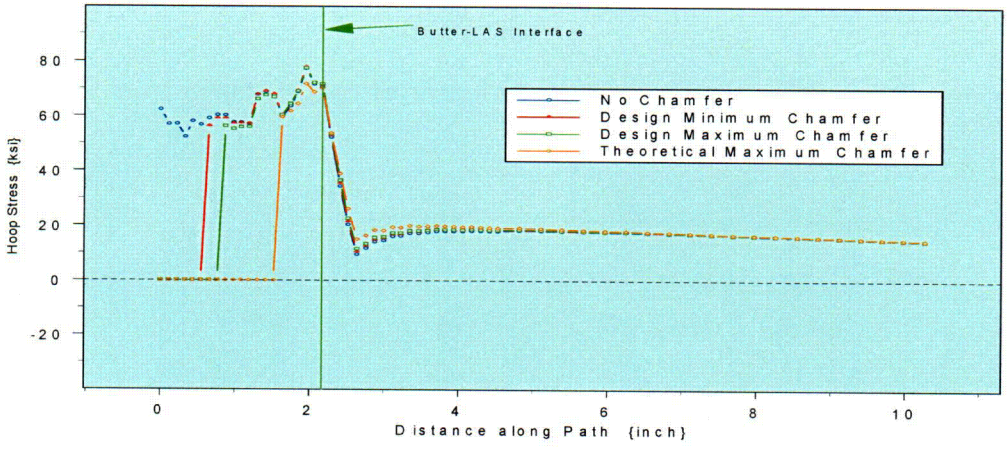

b) Steady State Condition

Figure 11: *Hoop stress distribution at the uphill location along the selected path. The J-groove weld corner is at the left (0.0) and the RVH OD at the right (10.27"). The hoop stress is highly localized to the J-groove weld region. The effect of steady state operation is to soften the peak residual stress in the J-groove weld and eliminates the compression region immediately beyond the interface between the butter and the RVH. The effect of the chamfer design on the peak magnitude appears to be minimal. The location of the butter to RVH interface is shown by the green vertical line, which is located at 2.17 inches from the corner.*

The stress contours shown in Figures 4 through 7 and the hoop stress plots along the selected path shown in Figures 10 and 11 show the following:

C12

Technical Report to Support Relief Request ANO1-R&R-006

1) The residual stress magnitude in the J-groove weld after the installation of various chamfer designs remains high.
2) There is some reduction of the total stress magnitude in the J-groove weld under steady state operating condition. This may be attributed to the bore hole dilation due to head expansion that occurs in this condition. However, it is important to note that the total stresses are dominated by the residual stress component.
3) The high hoop stresses are limited to the J-groove weld and to the vicinity of the buttering and the RVH base metal at the uphill and downhill locations. The remaining portion of the RVH has a much lower stress level.
4) The stress distributions at circumferential locations in between the uphill and downhill locations are much lower in magnitude (Figures 4 through 7). Hence the two locations for a bounding fracture mechanics analysis are the uphill and downhill locations.
5) Significant reduction in the stresses was not observed in the J-groove weld and its immediate vicinity for the various chamfer design simulations.

In order to assess the impact of residual stress on the total operating stress distribution, a comparison between the steady state conditions for the "design maximum chamfer" case from this evaluation was compared to the steady state operating stress obtained from Reference 1. In Reference 1 the steady state operating stress distribution does not include the residual stress component. This comparison is presented in Figure 12. In this figure, a third order polynomial fit to the stress data is also shown.

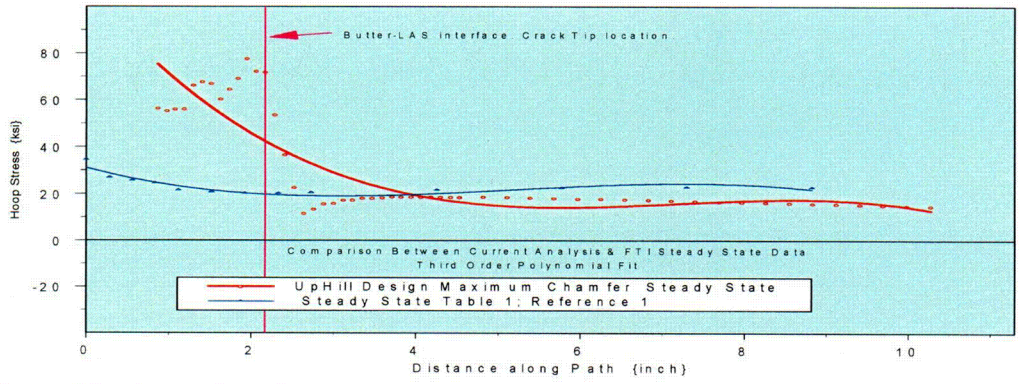

Figure 12: *Comparison between current analysis and that from Reference 1 for steady state condition at the uphill location. The current analysis is dominated by residual stress that results in a higher stress magnitude in the J-groove weld. The third order polynomial does not adequately represent the stress distribution of the current analysis. Ignoring the residual stress contribution results in a much lower magnitude stress distribution in the J-groove weld region.*

Technical Report to Support Relief Request ANO1-R&R-006

The following inferences can be made from Figure 12:

1) The third order polynomial does not adequately fit the data from the current analysis. Fracture mechanics analysis using closed form weight function methods, currently available, use a third order polynomial fit to describe the stress distribution; hence, using these formulations would introduce a significant error in the estimation of the SIF.
2) Fracture mechanics closed form solutions that use far field stresses necessitate linearizing the stress distribution. For the current application such a linearization would result in a high value for the membrane stress component, which would lead to an unrealistically high SIF.
3) Fracture mechanics analysis using closed form solutions cannot properly account for the highly localized stress distribution. Hence, the use of such solutions will not accurately characterize the prevailing SIF at the butter to RVH interface. The only rational alternative is to perform finite element-based fracture mechanics analysis.
4) The significant contribution of residual stress, in the region of interest, cannot be ignored. If the residual stress contribution to the SIF is not considered, the SIF would be severely underestimated. This aspect is explored further in the section titled "Discussion".

The numerical results from the stress analysis for the cases evaluated were transmitted electronically to the vendor performing the fracture mechanics analysis. The fracture mechanics analysis is discussed in the following section.

Technical Report to Support Relief Request ANO1-R&R-006

Fracture Mechanics Analysis

Conceptual Basis

The fracture mechanics analysis consisted of two separate steps:

1) Determine SIF along the crack front for the various imposed loads.
2) Perform a fatigue crack growth analysis.

For the determination of SIF, the finite element model developed for the residual stress analysis was modified to incorporate a fine mesh distribution in the region of interest (in the region where the crack was modeled). In the modified model the appropriate loading condition was simulated by a crack face pressure, which corresponded to the stress in the same region that was developed in an un-cracked structure upon imposition of the desired load. This method follows from the principle of superposition to determine the SIF, which can be described as follows [10]:

1) Sketch "a" shows the remote loading for an un-cracked plate; sketch "b" shows the same plate but with a central through-wall crack that is remotely loaded in tension and the crack is loaded in compression by a stress magnitude such that the crack is closed. These two loading conditions can be split as an algebraic sum of sketches "c" and "d" as depicted in Figure 13.

2) From the principle of superposition it can be shown that;
$K_{sketch\ "b"} = K_{sketch\ "c"} + K_{sketch\ "d"} = 0$ *(un-cracked plate)*
Therefore, $K_{sketch\ "c"} = -K_{sketch\ "d"} = \sigma\sqrt{\pi a}$ *(center cracked panel)*
Or, $K_{sketch\ "d"} = -\sigma\sqrt{\pi a}$
When the crack face is pressurized by a pressure "p" which is equal and opposite of the remote stress "σ" then, $K_{sketch\ "d"} = p\sqrt{\pi a}$.

3) The principle of superposition applies only to the region that is dominated by the stress singularity, which is in the immediate vicinity of the crack.

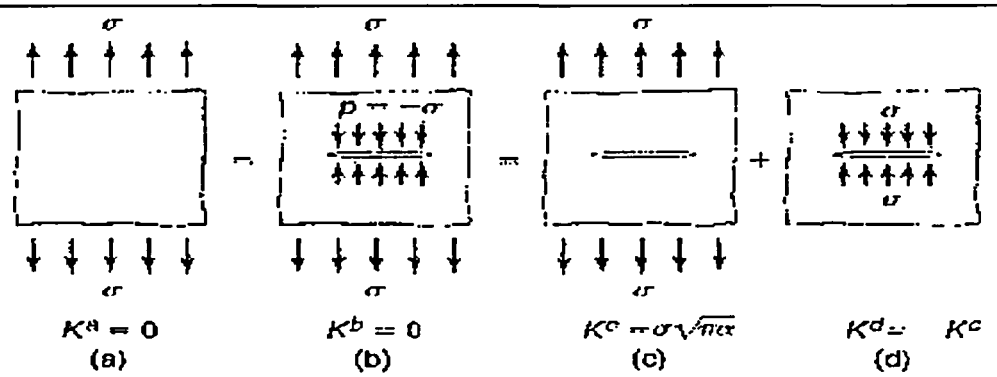

Figure 13: *Determination of SIF for a pressurized center crack using the principle of superposition [10]. From the individual sketches the following can be defined [10]:*
$K^b = 0 = K^c + K^d$; *hence* $K^c = -K^d$;
Since $K^c = \sigma\sqrt{\pi a}$, *and the crack face pressure is equal and opposite to the remote tension stress the SIF for sketch "c" becomes* $K^c = p\sqrt{\pi a}$

Technical Report to Support Relief Request ANO1-R&R-006

The determination of SIF using finite element modeling method required special crack tip elements, which are located along the entire crack front. The crack tip elements were three-dimensional brick elements that had the mid-side nodes moved to the quarter point to simulate the proper singularity condition that exists at the crack tip.

Determination of Stress Intensity Factor

The assumed crack was modeled with a significantly refined mesh than that used in the stress analysis. A total of 50 nodes were used to define the crack front. Of these 50 nodes, 42 nodes represent crack between the low alloy steel and the buttering layer. The mid-side nodes of the crack front elements are moved to the quarter point location such that the singularity at the crack tip is maintained. Note that the first node is at the ID of the CRDM bore and the last fifty first node is at the RVH cladding wetted surface.

The chamfer design, which was shown in Figure 2, was modeled as follows:

1) The entire remnant J-weld including the butter weld was assumed to be cracked.
2) The flaw is modeled both on the uphill and downhill J-weld.
3) The hoop stresses obtained from the residual stress analysis, for an un-cracked geometry at the location of the remaining crack, was used to develop the crack face pressures for the radial-axial crack.
4) The internal pressure was modeled as crack face pressure and applied to the no chamfer case only. The resulting SIF for the internal pressure was added to the steady state SIF for the other cases. This approach is considered to be conservative, since, the SIF due to the internal pressure is maximized.
5) The intact regions are modeled with symmetry boundary conditions that represent material and geometric continuity.

The finite element model of the flaw geometry, including the loading applied to the crack face is shown in Figure 14 for the "no chamfer case". The SIF at all the crack tip locations were determined using the finite element post processing routine. The SIF at all locations, including those in the cladding were determined. Since a portion of the assumed crack is located at the J-groove weld to the stainless steel cladding interface (8 nodes from the cladding end), the SIF for these locations need not be considered for the evaluation of non-ductile failure. Therefore, the maximum SIF used in the evaluation with respect to the allowable fracture toughness prescribed in Reference 8 were from the nodes located on the low alloy steel interface with the buttering layer. The allowable SIF for the carbon steel was calculated based on upper shelf toughness, and the specification of IWB-3613(b) and IWB-3613(c) of Reference 8, are as follows:

Technical Report to Support Relief Request ANO1-R&R-006

Normal and Upset conditions {IWB-3613(b)}: 63.25 ksi$\sqrt{in}$.
Emergency and Faulted condition {IWB-3613(c)}: 141.44 ksi$\sqrt{in}$.

The fracture mechanics analysis for the various cases considered was performed as follows:

1) No Chamfer: The as-counterbored condition was analyzed for the steady state, residual stress only, and the internal pressure acting on the crack face. This represented a base case for comparison purposes and was used to obtain a conservative estimate of SIF due to crack face pressure. The specific case for the internal pressure acting on the crack face provides a maximum SIF because the force created by the internal pressure is a maximum for this case. The chamfer cases, which have a lower crack face area, the force due to the internal pressure acting on the crack face would be lower than that for the no chamfer case. The SIF obtained from this case was added to the steady state SIF for the other cases as needed.
2) Design Minimum Chamfer: Only steady state and residual stress only loadings were evaluated for this case. Transient operating stresses were evaluated for the maximum design chamfer case.
3) Design Maximum Chamfer: The SIF were calculated for the steady state, residual stress, and the four transient conditions considered in the stress analysis. A comparison of the results between the steady state and the transient conditions showed that the SIF for the transient condition were very close to that from the steady state condition, due to the predominant contribution of the residual stress component. Hence, it was not necessary to calculate the SIF for the transients for each of the chamfer conditions analyzed.
4) Theoretical Maximum Chamfer: Only steady state and residual stress conditions were analyzed. This geometry was analyzed to evaluate the effect of varying chamfer size on the resulting SIF.

No Chamfer Case

This geometry provides a base case for the comparison of the SIF as it relates to the chamfer size. This case also provided the opportunity to obtain a conservative upper bound for the SIF owing to the internal pressure acting on the crack face. The finite element model showing the application of crack face pressure based on the residual stress and steady state conditions are presented in Figure 14. The crack face pressure is simulated on the entire region that is assumed cracked (i.e. J-groove weld and buttering layer). The remaining region, which is not cracked, has no pressure application. The crack tip nodes are along the crack front between the buttering and RVH interface (between the white arrows along the RVH boundary). In other cases (figures) the crack front is

Technical Report to Support Relief Request ANO1-R&R-006

located along the boundary shown in Figure 14 and, hence, not shown in the other figures.

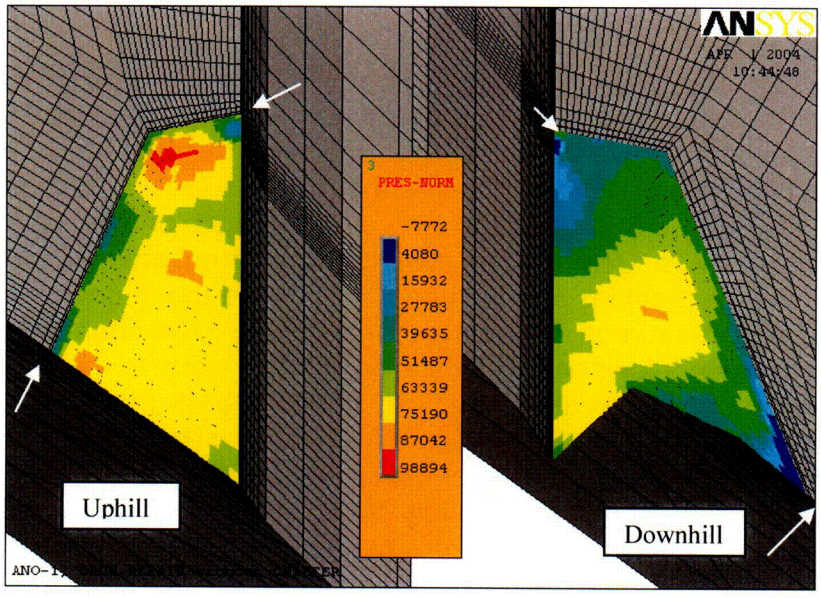

a) Residual Stress Loading Only

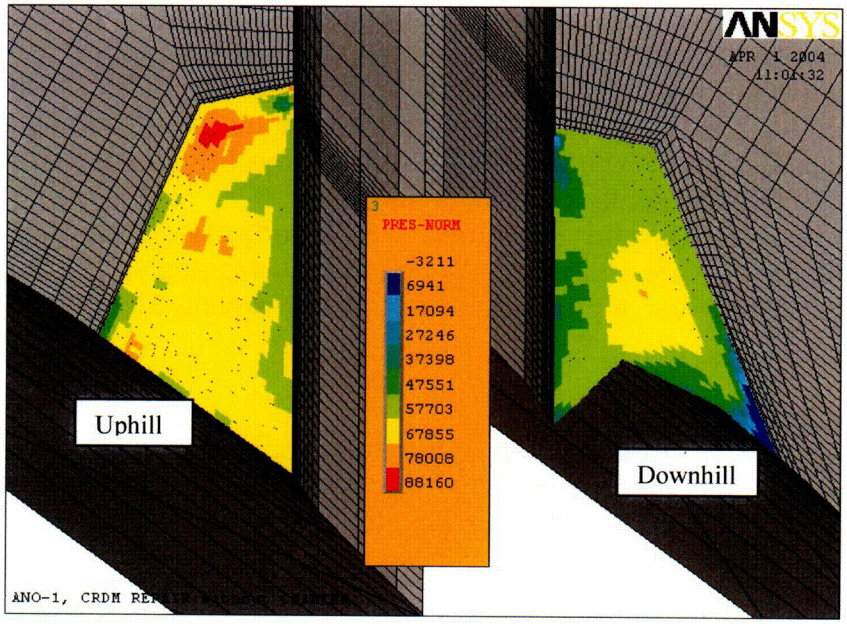

b) Steady State Loading

Figure 14: *Finite element fracture mechanics model for the no chamfer case. The residual loading is shown in "a" and the steady state loading in "b". A small compressive zone on the downhill crack where it intersects the RVH cladding is observed.*

Technical Report to Support Relief Request ANO1-R&R-006

The steady state loading tends to make the stress distribution more uniform and increases the magnitude (color change). The SIFs for this case are shown in Figure 15.

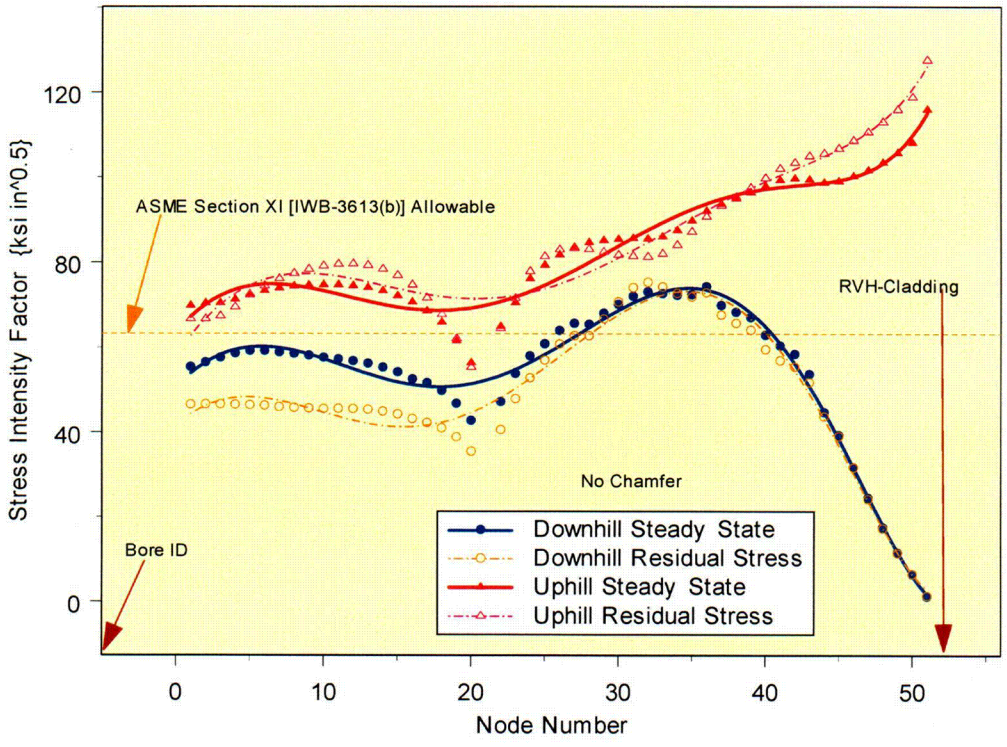

Figure 15: *SIF plot for the no chamfer case. The SIF due to residual stress (open symbol) and steady state condition (closed symbol) for both the uphill and downhill cracks are shown. A sixth order polynomial fit to the data is also shown. Significant difference between the residual stress and steady state condition is not observed.*

From Figure 15 the following observations are made:

1) The SIF for the uphill crack is higher than that for the downhill crack.
2) There is no significant difference between the SIF for the residual stress and steady state condition. This indicates that the residual stress distribution is the major contributor to the SIF.
3) The ASME Section XI allowable [8] is exceeded for certain locations along the crack front on the downhill side and for all locations on the uphill side.

4) The upper end of the crack, where the crack intersects the bore ID is on the left end of the graph. The right end of the graph is the location of the interface between the assumed flaw tip that is located between the buttering and the RVH-cladding on the wetted surface of the RVH. The node numbers representative of the crack front interface with the low alloy steel extends from node number 1 to node number 43.

5) A sixth order polynomial fit provides a reasonable approximation of the SIF distribution along the crack front. At the location of the transition of the J-weld prep knee, a sharp drop in the SIF data (individual points) occurs whereas the fitted line shows a smoother drop. The knee of the weld prep was approximated in the model and resulted in a sharp corner, which may be the reason for the sharp drop. However, the fitted line smoothes out the drop and may be more representative of the actual geometry.

Design Minimum Chamfer Case

This case represents the chamfer that could be installed following the minimum dimensions provided in Reference 9. The crack face loadings for this case are shown in Figure 16. The chamfer on the uphill is visible but on the downhill the chamfer is very small and is barely noticeable in the figure.

Technical Report to Support Relief Request ANO1-R&R-006

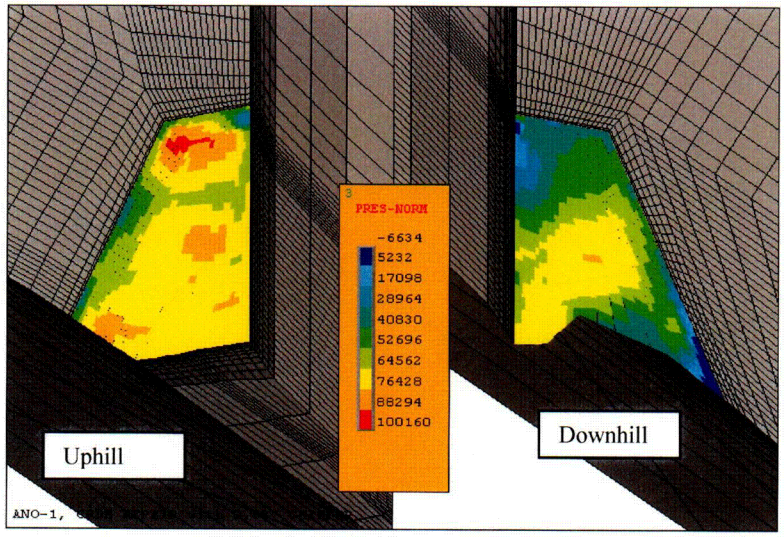

a) residual Stress Loading Only

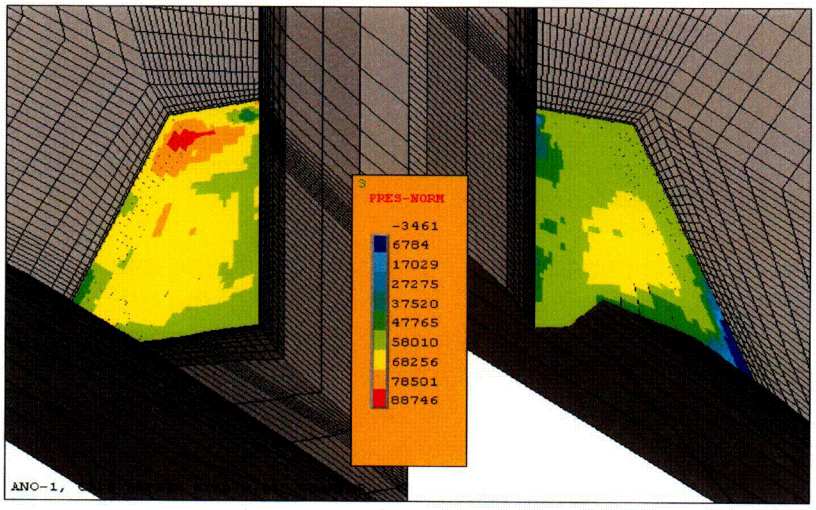

b) Steady State Loading

Figure 16: *Finite element fracture mechanics model for the design minimum chamfer case. The residual loading is shown in "a" and the steady state loading in "b". A small compressive zone on the downhill crack where it intersects the RVH cladding is observed.*

Figure 16 shows similar features to those in Figure 14. The SIF for the minimum design chamfer case are presented in Figure 17.

Technical Report to Support Relief Request ANO1-R&R-006

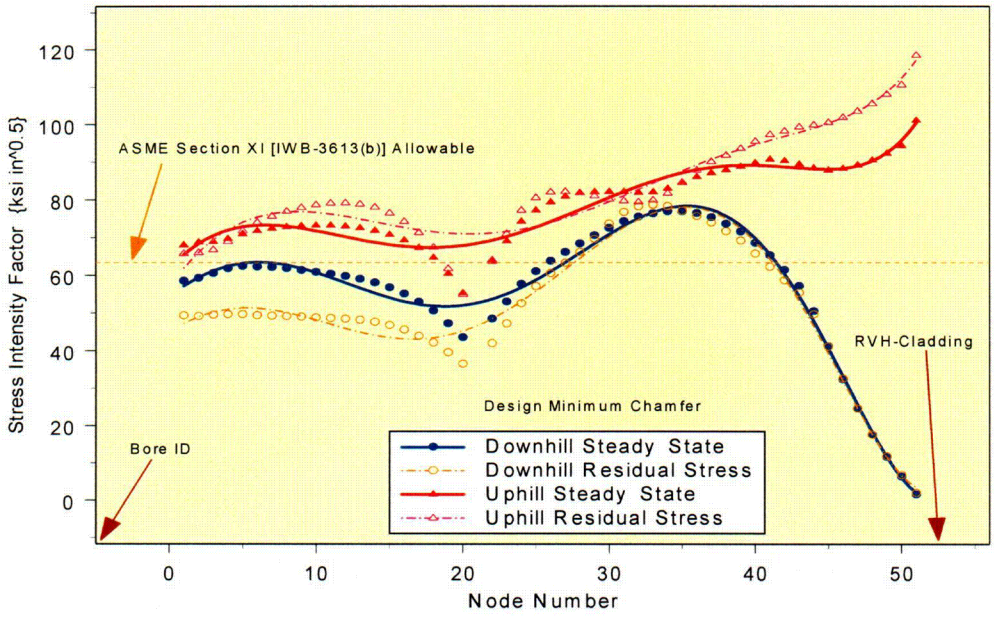

Figure 17: *SIF plot for the design minimum chamfer case. The SIF due to residual stress (open symbol) and steady state condition (closed symbol) for both the uphill and downhill cracks are shown. A sixth order polynomial fit to the data is also shown. Significant difference between the residual stress and steady state condition is not observed.*

The node description for this case is similar to the information provided in item four (4) in the no chamfer case. The behavior of the SIF distribution in Figures 15 and 17 are very similar. Hence, the same observations, made from Figure 15 apply to Figure 17. The magnitude of the SIF is slightly different between the two figures. For the downhill crack there appears to be a slight increase and for the uphill crack a slight decrease when compared to Figure 15 (no chamfer case).

Design Maximum Chamfer Case

This case represents the chamfer that could be installed following the maximum dimensions provided in Reference 9. The crack face loadings for this case are shown in Figure 18. The chamfer on the uphill is visible, but on the downhill, the chamfer is small and is barely noticeable in the figure.

Technical Report to Support Relief Request ANO1-R&R-006

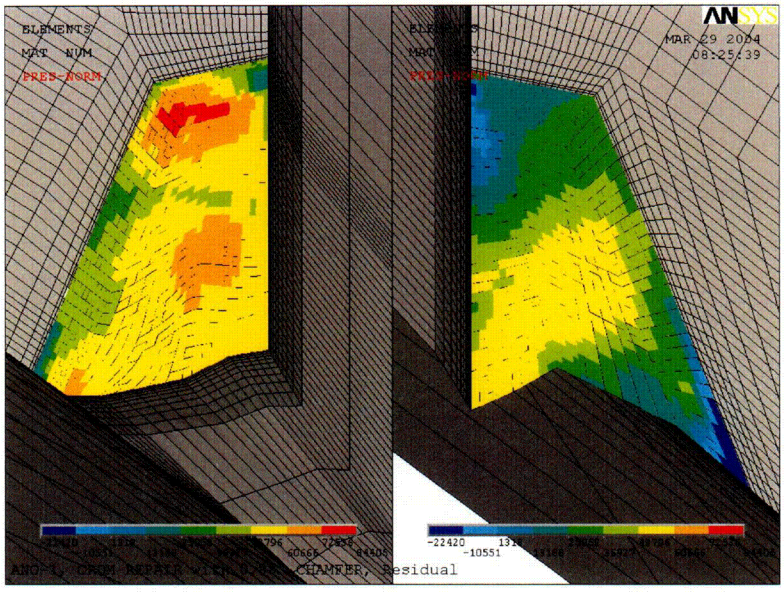

a) Residual Stress Loading Only

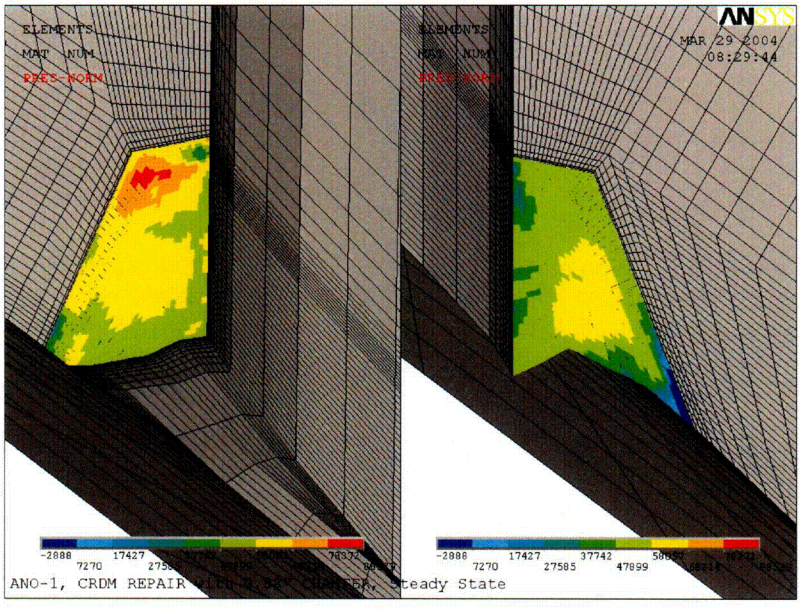

b) Steady State Loading

Figure 18: *Finite element fracture mechanics model for the design maximum chamfer case. The residual loading is shown in "a" and the steady state loading in "b". A small compressive zone on the downhill crack where it intersects the RVH cladding is observed.*

Figure 18 shows similar features to those in Figure 14. The SIF for the minimum design chamfer case are presented in Figure 19.

C18

Technical Report to Support Relief Request ANO1-R&R-006

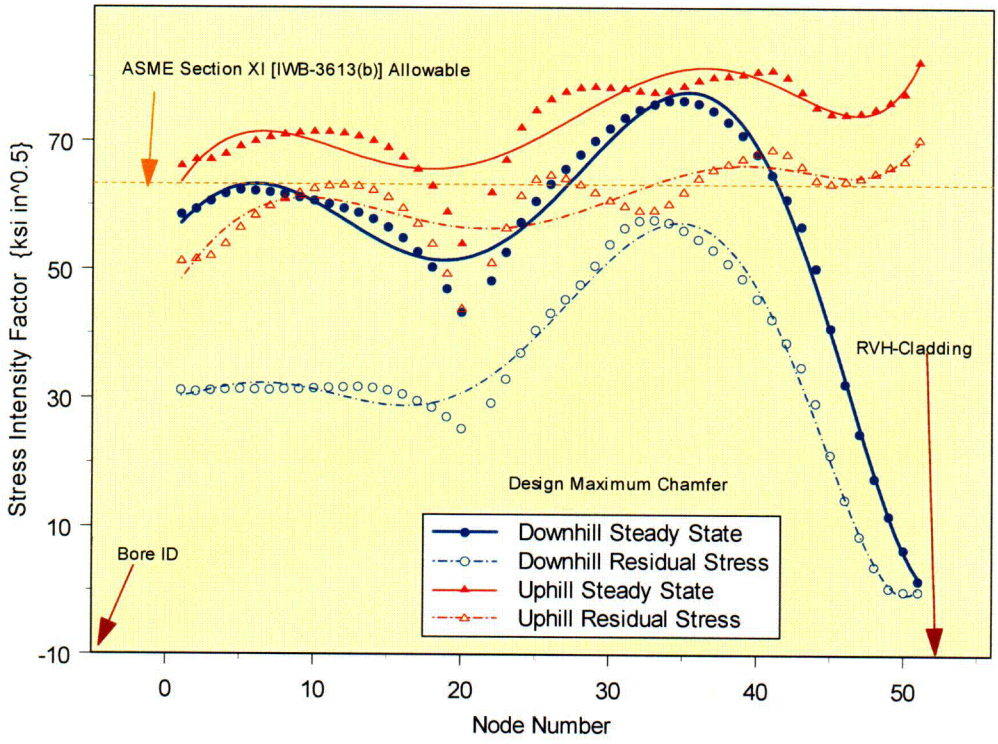

Figure 19: *SIF plot for the design maximum chamfer case. The SIF due to residual stress (open symbol) and steady state condition (closed symbol) for both the uphill and downhill cracks are shown. A sixth order polynomial fit to the data is also shown. Though a difference between the residual stress and steady state condition is observed, the SIF at some crack locations exceed the ASME Section XI allowable.*

The node description for this case is similar to the information provided in item four (4) in the no chamfer case. The behavior of the SIF distribution in Figures 15 and 19 are similar. Hence, the same observations made from Figure 15 apply to Figure 19. The magnitude of the SIF is slightly different between the two figures. For the downhill crack there appears to be a slight increase and for the uphill crack a slight decrease when compared to Figure 15 (no chamfer case). Though there is a reduction in the SIF magnitude compared to the no chamfer case, the SIF at some crack front locations were found to exceed the allowable value of ASME Section XI IWB-3613(b) [8].

Theoretical Maximum Chamfer Case

This case was evaluated to ascertain the maximum theoretical benefit of installing a chamfer on the J-groove weld remnant. The model, as shown in Figure 2, removes a major portion of the J-groove weld remnant on the

Technical Report to Support Relief Request ANO1-R&R-006

uphill side. The remnant on the downhill side is removed by following the contour along the periphery of the weld as rotated from the uphill towards the downhill side. However, this theoretical maximum chamfer cannot be installed in the field since it would require extensive tooling modification and testing. Therefore, the evaluation of this concept was to ascertain whether or not a theoretical maximum removal would enable satisfying the allowable limit of the ASME Section XI, IWB-3613(b) [8]. The finite element model for the SIF determination is shown in Figure 20.

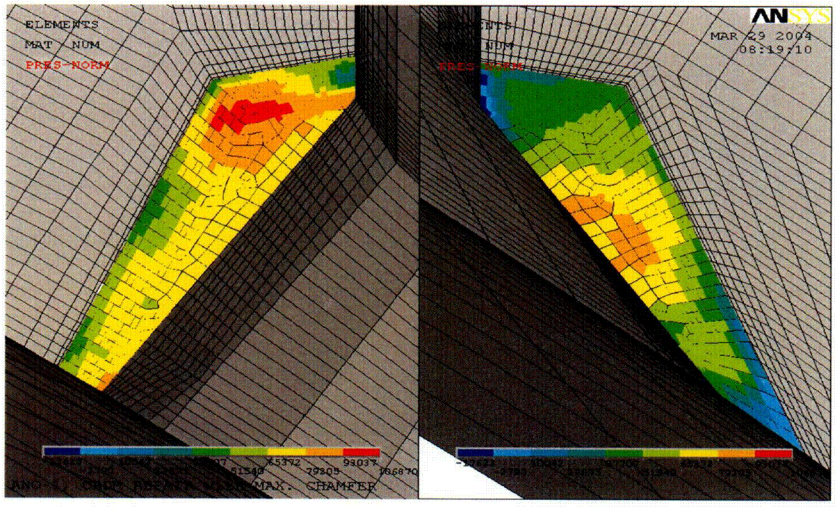

a) Residual Stress Loading Only

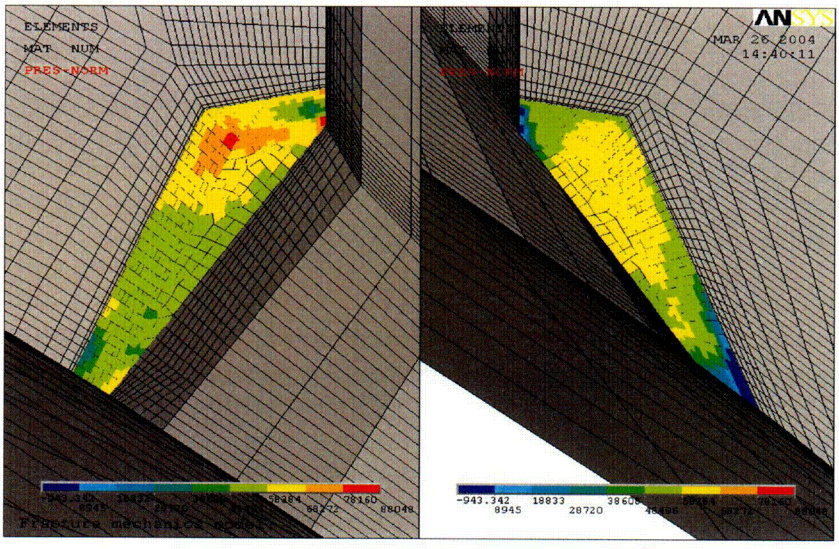

b) Steady State Loading

Figure 20: *Finite element fracture mechanics model for the theoretical maximum chamfer case. The residual loading is shown in "a" and the steady state loading in "b". A small compressive zone on the downhill crack where it intersects the RVH cladding is observed.*

Technical Report to Support Relief Request ANO1-R&R-006

Figure 20 shows similar features to those in Figure 14. The SIF for the minimum design chamfer case are presented in Figure 21.

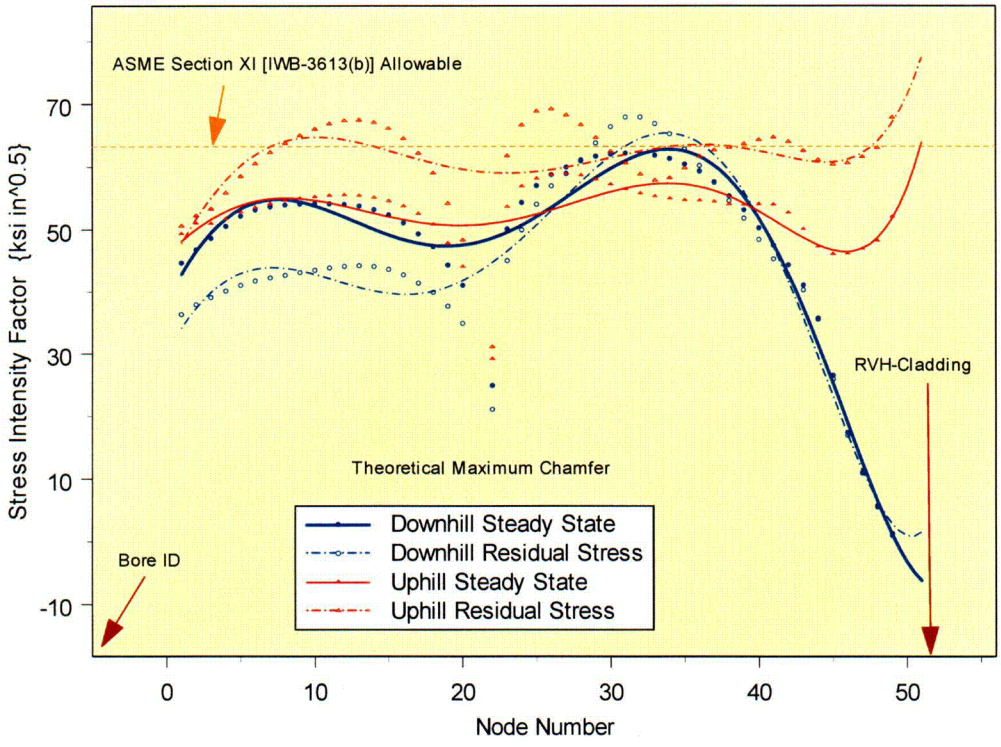

Figure 21: *SIF plot for the theoretical maximum chamfer case. The SIF due to residual stress (open symbol) and steady state condition (closed symbol) for both the uphill and downhill cracks are shown. A sixth order polynomial fit to the data is also shown. Though a difference between the residual stress and steady state condition is observed, the SIF at the downhill crack location for the steady state condition exceeds the ASME Section XI allowable.*

The node description for this case is similar to the information provided in item four (4) in the "no chamfer case". The behavior of the SIF distribution in Figures 15 and 21 are similar. Hence, the same observations made from Figure 15 apply to Figure 21. The magnitude of the SIF is slightly different between the two figures. Though there is a reduction in the SIF magnitude compared to the no chamfer case, the SIF at some downhill crack front locations, for the steady state condition, were found to exceed the allowable value of ASME Section XI IWB-3613(b) [8].

Internal Pressure Applied to Crack Face

The application of the reactor coolant system (RCS) internal pressure was analyzed as a separate case using the "no chamfer model". The no chamfer

CZ1

Technical Report to Support Relief Request ANO1-R&R-006

model has the highest crack face area; hence, the SIF resulting from the application of the internal pressure on the crack face will be maximized. The SIF obtained from this analysis was added to the respective steady state solutions from the three chamfer cases. In Figure 22 for the "no chamfer case", the effect of applying the RCS internal pressure on the crack face is shown. The SIF from the steady state analysis is presented for comparison. The impact of considering the RCS pressure on the crack face is evident as it shows a noticeable increase in the SIF.

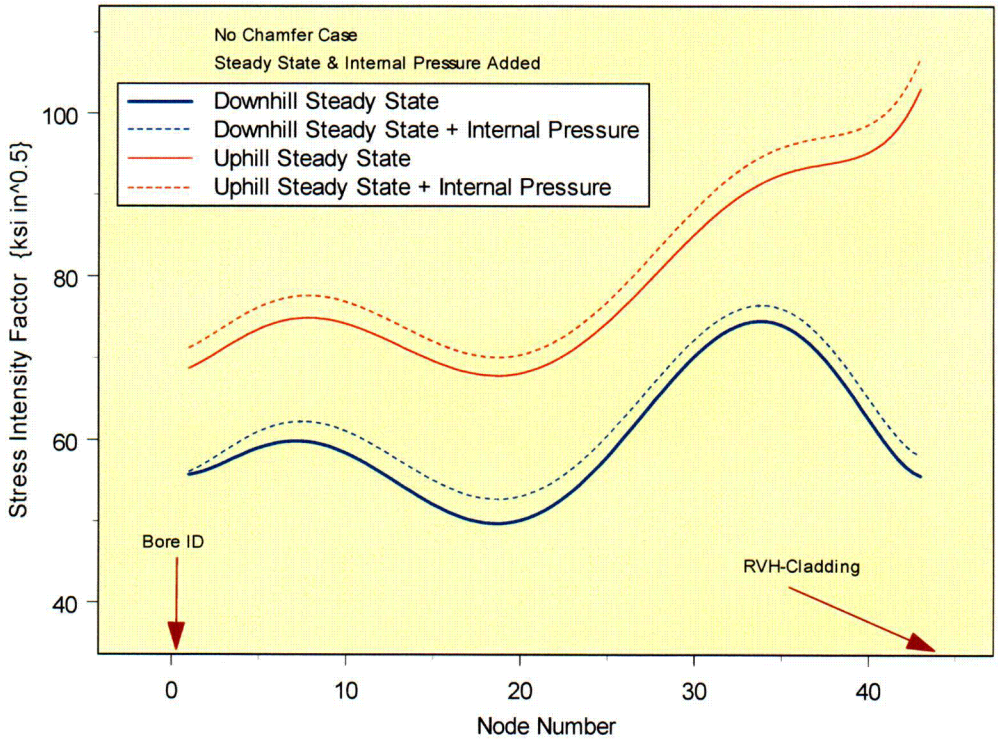

Figure 22: *Effect of RCS pressure on no chamfer case. The RCS pressure when added to the crack face results in an increase in the SIF. The solid lines are for the total SIF (Residual + Operating + RCS pressure on Crack face) and the broken lines for the steady state case (Residual + Operating).*

The SIF obtained for the RCS pressure on the crack face from the analysis of the no chamfer case was added to the steady state (residual + operating) results for the three chamfer cases. In Figures 23 and 24, the results for the total SIF (Residual + Operating + RCS pressure on crack face) for the three chamfer cases are presented and compared to the ASME Section XI, IWB-3613(b) [8] allowable value. Figure 23 presents the result for the crack centered

C22

Technical Report to Support Relief Request ANO1-R&R-006

at the downhill location and Figure 24 for the crack centered at the uphill location. From these two figures it is observed that the ASME Section XI allowable is exceeded either for both crack locations (design chamfer) or at the downhill location for the theoretical maximum chamfer. This result shows that chamfering to reduce the J-weld remnant size does not result in an acceptable SIF.

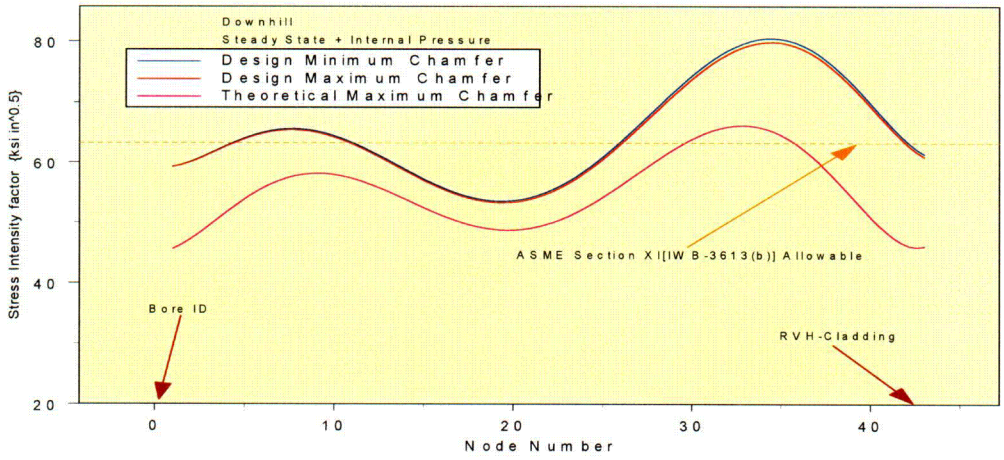

Figure 23: *Comparison of total SIF for the three chamfer cases at the downhill location. There appears little difference between the two design chamfer cases (minimum and maximum); because the size of the chamfer at the downhill location for both cases were very small when compared to the uphill side. The SIF for the theoretical maximum chamfer is also found to exceed the ASME Section XI allowable.*

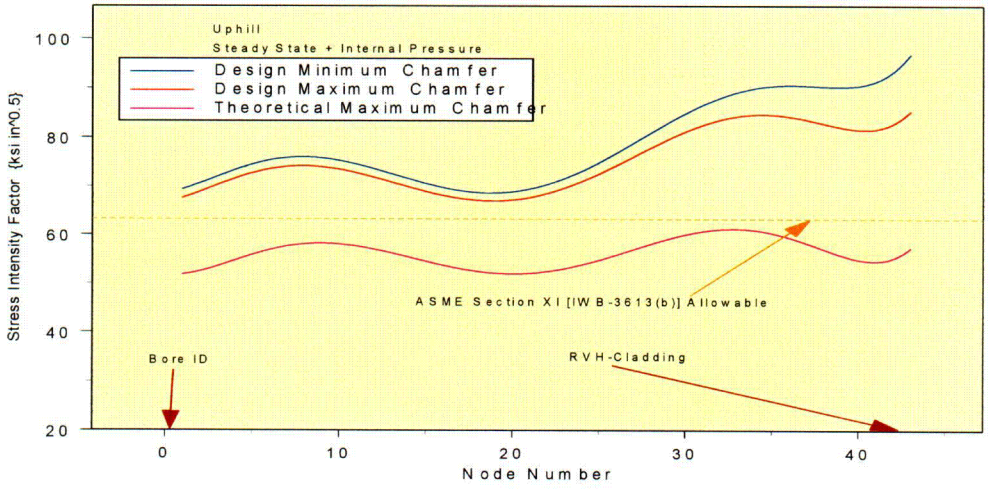

Figure 24: *Comparison of total SIF for the three chamfer cases at the uphill location. A reduction in the SIF from the design minimum to theoretical maximum chamfer is observed. Neither of the design chamfers meets the ASME Section XI allowable.*

C23

Technical Report to Support Relief Request ANO1-R&R-006

The fracture mechanics analysis method, presented above, conforms to the NRC expectation of Reference 11. The results for the maximum SIF along the crack front interface with the low alloy steel RVH is presented in Table 1. The SIF values that were above the ASME Section XI allowable [8] are shown in red font.

Table 1 : Maximum SIF from Fracture Mechanics Analysis

J-groove Weld Remnant Configuration	Maximum Applied Stress Intensity Factor[1] (ksi√in)		
	Steady State Operation[2]	Residual Stresses Only[3]	Operating Condition Only[4]
No Chamfer	**77.4** – Downhill **103.4** - Uphill	**75.3** – Downhill **105.0** – Uphill	2.1-Downhill Note 5 – Uphill
Design Minimum Chamfer	**80.0** –Downhill **94.4** - Uphill	**78.6** – Downhill **99.3** – Uphill	1.4 – Downhill Note 5 – Uphill
Design Maximum Chamfer	**79.4** – Downhill **84.8** - Uphill	57.8 – Downhill **68.7** – Uphill	21.6 – Downhill 16.1 Uphill
Theoritical Maximum Chamfer	**65.2** – Downhill 62.5 - Uphill	**67.9** – Downhill **69.1** – Uphill	Note 5 –Downhill Note 5 - Uphill

Notes:

1) *The applied SIF is based on considering the three conditions provided in 2, 3, and 4 below.*
2) *The steady state condition is the combined SIF based on residual stress plus the steady state operating stresses (pressure and temperature).*
3) *The residual stress condition is based on the residual stress state after completion of the specific operation on the J-groove weld as indicated by the configuration column.*
4) *The operating condition is the difference between the steady state condition and the residual stress state. This column provides the SIF estimate due to the operating condition alone.*
5) *The SIF due to the residual stress is higher than at steady state operating condition.*

The results presented in Table 1 show that for most of the cases evaluated the maximum SIF exceeds the ASME Section XI allowable [8] value of 63.2 ksi√in.

Analysis of Transients

The transient analysis was performed on the design maximum chamfer geometry, because the fracture mechanics analysis results showed that there were very small differences in the SIF between the two chamfer designs (minimum and maximum). The transients considered, which were based on References 1 and 12, were as follows:

1) Heat-up {Normal & Upset condition}.
2) Cooldown {Normal & Upset condition}.
3) Reactor Trip {Normal & Upset condition}.

Technical Report to Support Relief Request ANO1-R&R-006

4) Inadvertent Rod Withdrawal {Accident/Faulted condition}.

The SIF results from the transient analysis are compared with the corresponding steady state SIFs, which are presented in Figure 25 for the downhill location and Figure 26 for the uphill location.

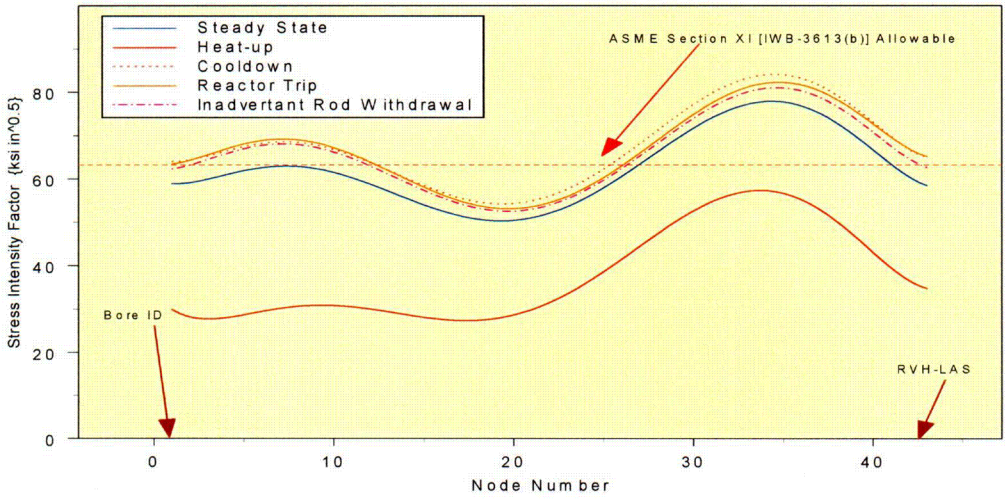

Figure 25: *Results for transient analysis for the design maximum chamfer case at the downhill location. The cooldown, reactor trip, and the rod withdrawal transient SIF are slightly higher than that for the steady state condition. The distribution of the SIFs is very similar.*

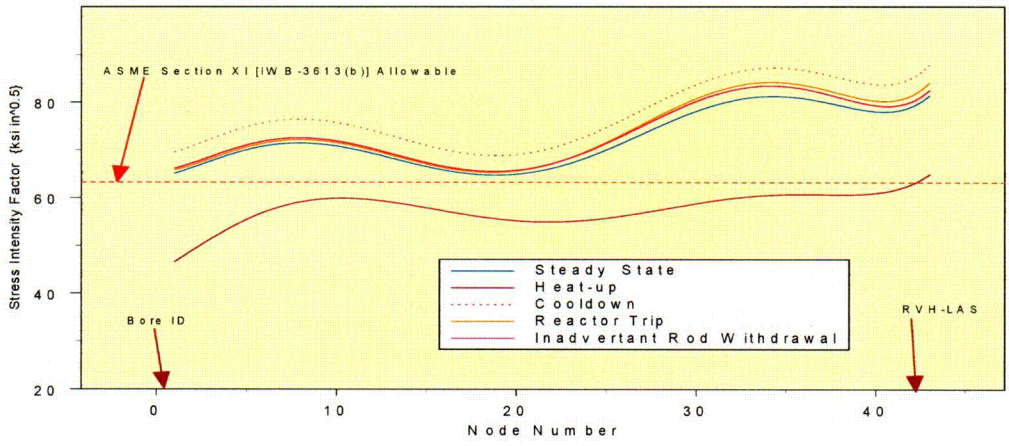

Figure 26: *Results for transient analysis for the design maximum chamfer case at the uphill location. The cooldown, reactor trip, and the rod withdrawal transient SIF are slightly higher than that for the steady state condition. The distribution of the SIFs is very similar.*

C24

Technical Report to Support Relief Request ANO1-R&R-006

The results from the transient analysis, presented in Figures 25 and 26, indicate that the SIF during some of the transients are slightly higher than the steady state condition. The SIF for the two transients representing the normal and upset condition (Heat-up/cooldown and reactor trip) are the transients that would impose a fatigue loading at the crack tip. These transient results will be used to perform the fatigue crack growth analysis. The uphill location SIFs are higher than those at the downhill location. For the two transients that represent the normal and upset condition, the SIF are found to exceed the ASME Section XI allowable [8] for that condition. The inadvertent rod withdrawal is an accident condition and the resulting SIF is within the ASME Section XI allowable for accident condition [8].

Fatigue Crack Growth Analysis

The fatigue crack growth was computed from the transient analysis results described above. The fatigue crack growth was performed for one cycle of operation. The number of transient events was obtained form References 1 and 12. The transients considered for the fatigue crack growth were as follows:

1) Normal Heat-up/Cooldown - 6 cycles/year
2) Reactor Trip/Heat-up - 6 cycles/year

The fatigue crack growth law for light water environment presented in Appendix "A" in ASME Code, Section XI [8], was used for this evaluation. From the transient data presented for the uphill crack the maximum "ΔK" was found to be as follows:

1) Normal Heat-up/Cooldown - 38.7 ksi$\sqrt{in}$.
2) Reactor Trip/Heat-up - 39.2 ksi$\sqrt{in}$.

The constants for the fatigue crack growth equation were based on "ΔK" and the "R" ratio (K_{max}/K_{min}) which was 0.43. Based on these values the material constant "n" and the scaling constant "C_0" were as follows:

1) Material constant "n" = 1.95 (Paragraph A-4300 of Reference 8)
2) Scaling constant "C_0" = 1.179×10^{-7} (Paragraph A-4300 of Reference 8)

The fatigue crack growth for one cycle of operation showed the growth to be 0.005 inch. The extent of fatigue crack growth is very small and would not impact the SIF significantly. Therefore, the need to determine the end-of-operating cycle based SIF would not be necessary.

Technical Report to Support Relief Request ANO1-R&R-006

Discussion:

Consideration of Residual Stress

The impact of residual stress on fracture behavior is succinctly presented in Reference 13. In the work presented it was shown, by detailed analysis and experimental testing, that residual stress resulting from welding alters the constraint at the crack tip and simultaneously affects the crack driving force. The analytical effort included detailed finite element analysis and micromechanical modeling. The experimental effort included fracture mechanics testing. The results of the various evaluations showed that the influence of residual stresses was much greater for brittle fracture than for ductile fracture. The importance of adequate representation of the residual stress field to assess fracture conditions was demonstrated.

The work presented in Reference 13 clearly demonstrates the significance of residual stress in the fracture analysis of welded structures. Therefore, it is imperative that residual stress be properly accounted for in the fracture mechanics analysis using LEFM methods. When residual stresses are not considered, by increasing the flaw size such that the residual stress field becomes insignificant, the significant impact of residual stress on fracture (especially brittle fracture) is ignored. Such an analysis will not assess the true potential for brittle fracture and will provide a false margin against brittle fracture. Therefore, a proper and rigorous analysis to evaluate the margin against brittle fracture must adequately consider (and represent) the impact of residual stress.

ASME Code Consideration

The allowable SIF based on IWB-3613(b) [8] is 63.2 ksi$\sqrt{in}$ for an upper shelf fracture toughness of 200 ksi$\sqrt{in}$. As shown in the table, the applied SIFs are above the allowed minimum. The basis for the safety factor of "$\sqrt{10}$" in IWB-3613(b) can be found in Reference 14:

"The acceptance criteria of IWB-3611 on flaw size were developed with the original purpose of maintaining the design margins of Section III. It is well known that the nominal factor of safety for normal and upset conditions is 3. Consider the general relationship between the stress intensity factor and the stress and flaw size at failure based on linear-elastic fracture mechanics, as noted in the following equation:

$$K_{Ic} = \sigma\sqrt{\pi a}$$

where K_{Ic} = the fracture toughness.

It may therefore be deduced that a factor of safety of 3 on stress at failure is consistent with a factor of safety of 9 on flaw size. Code committees tend to

Technical Report to Support Relief Request ANO1-R&R-006

prefer round numbers, so the value of 9 is rounded up to 10 to provide a safety factor slightly higher than the design safety factor."

Therefore, the safety factor on the SIF, based on the above equation, results in a value of $\sqrt{10}$. The design safety factor value of 3 was based on the ultimate tensile strength of the ferritic material [15], thereby limiting the allowable general primary membrane stress (P_m) to be less than or equal to one-third of the material ultimate strength.

In addition the design rules for Section III of the ASME Boiler and Pressure Vessel Code are defined for primary bending stress (P_b) and local primary membrane stress (P_L) to be lower than $1.5S_m$, which is approximately equal to the material yield strength. Further, the stress range when considering secondary stresses is increased by an additional factor of two to $3S_m$. This increase for local primary stresses then results in a nominal safety factor of 2 with consideration of bending and local stress effects. The limit on secondary stresses was included to prevent gross distortion of Code components.

The aspect of using different safety factors based on loading type was recognized in Appendix G to ASME Section XI [8]. Although this appendix is for "hypothetical flaw analysis" to ensure safety against non-ductile fracture, its applicability to the evaluation of flaws potentially left in the CRDM J-groove welds is appropriate. The current evaluation assumes that the entire J-groove weld (including the butter) is cracked, which is analogous to postulating a maximum worse case hypothetical flaw. In particular the guidance provided in paragraph G-2222 (Consideration of Membrane and Bending Stresses) notes that; *"Equation (1) of G-2215 requires modification to include the bending stresses which may be important contributors to the calculated K_I value at a point near a flange or nozzle".* Therefore the controlling SIF equation, based on material toughness, was defined as:

$$K_{Ia} \geq 2(K_{Im} + K_{Ib})_{Primary} + (K_{Im} + K_{Ib})_{Secondary}$$

where:
K_{Ia} = *the available fracture toughness based on crack arrest for the corresponding crack tip temperature;*
K_{Im} = *the applied SIF due to membrane stress; and,*
K_{Ib} = *the applied SIF due to bending stress*

In Appendix G, the distinction between primary and secondary stresses are recognized by using a safety factor of 2 on primary stresses and not requiring a safety factor on secondary stresses.

The safety factor considerations in the Code (Section III and Appendix G of Section XI) are based on the through-wall stress distribution, which is also the consideration for IWB-3600 of Section XI [8]. However, the safety factor

Technical Report to Support Relief Request ANO1-R&R-006

presented in IWB-3613(b) considers the same safety factor for all stresses. This results in an overly conservative allowable SIF when the predominant loading mechanism is highly localized and due to residual stresses.

A more reasonable approach would be to utilize the philosophy of Appendix G to Section XI [8] and the safety factors utilized in Section III. This approach would result in the governing equation for SIF as:

$$K_{Ia} \geq 3.0(K_{Im} + K_{Ib})_{Primary} + 1.5\,(K_{Im} + K_{Ib})_{Secondary\ (or\ Residual)}$$

In the above equation the primary stresses would be those from operating pressure, which are the only non-displacement limited load on the top head. The secondary stresses would be those due to local structural discontinuity effects and thermal gradients. The safety factors applied are determined by multiplying those in Appendix G by a factor of 1.5. In this manner the appropriate safety margin against non-ductile fracture would be maintained in a manner similar to that prescribed by Appendix G but with a higher safety factor. However, as shown in Table 1, this approach would provide a safety factor of 1.5 since the stresses are shown to be predominantly those due to residual stresses.

As an alternative, a safety factor to be applied to the residual stresses can be deduced from the structure of the safety factor for primary bending and primary local membrane stresses defined in Section III. It was observed that the safety factor for these stresses was two-thirds of that for the general primary membrane stress. In addition the fracture mechanics analysis for the current evaluation demonstrates that the predominant loading is due to the localized residual stress distribution. Thereby, reducing the safety factor in IWB-3613(b) to 2. Thus the allowable SIF would be as follows:

$$K_{ITotal} \leq K_{Ia}/2$$

Using the results from the fracture mechanics analysis, for the maximum design chamfer case, the two approaches lead to the following result:

$$\text{Criteria 1: } K_{Ia} \geq 3.0(K_{Im} + K_{Ib})_{Primary} + 1.5(K_{Im} + K_{Ib})_{Secondary\ or\ Residual}$$

$$3(16.1)_{Operating\ Condition} + 1.5(68.7)_{Residual} = 151.4 \leq 200 \quad \text{Uphill Flaw}$$
$$3(21.6)_{Operating\ Condition} + 1.5(57.8)_{Residual} = 151.5 \leq 200 \quad \text{Downhill Flaw}$$

$$\text{Alternate Criteria } K_{ITotal} \leq K_{Ia}/2$$

$$2(84.8) = 169.6 \leq 200 \quad \text{Uphill Flaw}$$
$$2(79.4) = 158.8 \leq 200 \quad \text{Downhill Flaw.}$$

Technical Report to Support Relief Request ANO1-R&R-006

The examples provided above show that there is a significant margin against brittle fracture with either of the proposed acceptance criteria. In addition, the overall approach is conservative in that:

1. The fracture mechanics evaluation has been based on a hypothetical flaw that is assumed to exist in the entire J-groove weld.
2. The evaluation is based on linear elastic fracture mechanics principles with an assumed fracture toughness of 200 ksi$\sqrt{in}$. At elevated temperatures, the value of allowable fracture toughness is assumed, and the principles of elastic-plastic fracture mechanics, if used, could certainly demonstrate that significantly more margin would exist.

Significance of Reducing the Safety Factor

The stress analysis of the J-groove weld configuration demonstrated the hoop stress distribution was highly localized. This highly localized stress is not expected to cause general distortion of the RVH since the general membrane hoop stress is well within the Section III allowable limit. Therefore, a reduction in the safety factor from the current value of 3.16 [8] to the proposed alternate of 2.0 is reasonable. The impact of such a reduction on the limiting configuration (design minimum chamfer) is presented in Figure 27.

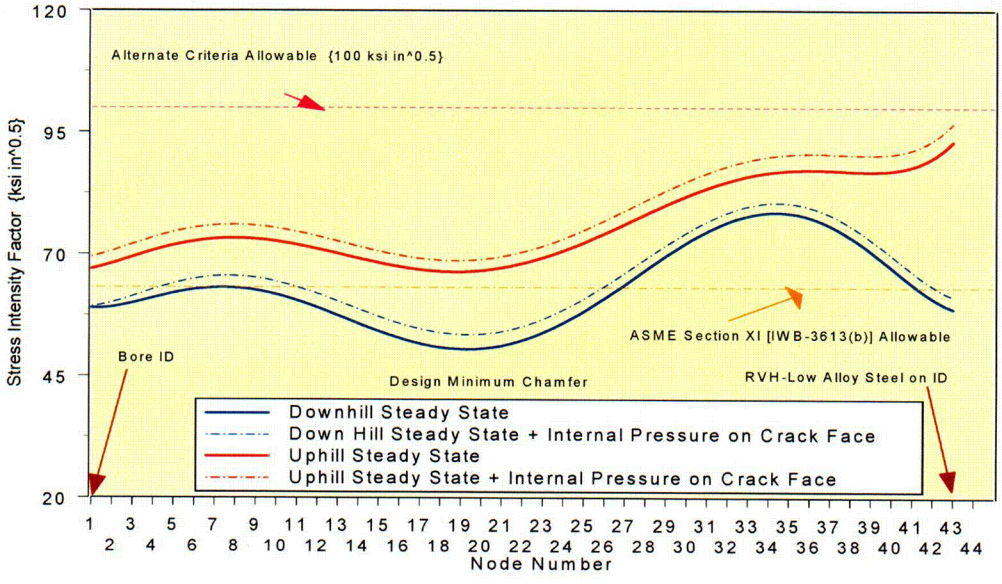

Figure 27: *Comparison of the impact of safety factor reduction. Total SIF (residual + operating + internal pressure) for the design minimum chamfer. The SIF exceeds the current ASME Section XI [IWB-3613(b)] allowable but is acceptable when the safety factor is reduced to 2.0.*

Technical Report to Support Relief Request ANO1-R&R-006

The results presented in Figure 27 demonstrate that the SIF, determined in accordance with the expectations of Reference 11, would not meet the current acceptance criteria [8]. However, the reduction of the safety factor, which would properly account for the highly localized stress distribution, shows that the prevailing SIF to be acceptable.

Conclusions

The analysis and discussions presented in this report support the following conclusions:

1) The stress distribution in the J-groove weld and its immediate vicinity is dominated by the residual stresses created by welding. These stresses are shown to be very localized and confined to the J-groove weld region.

2) The significance of considering residual stress has been demonstrated.

3) The stress distributions in the J-groove weld region are not amenable to characterization by either a third order polynomial or a linearized stress representation. This precludes the use of known empirical closed form solutions to estimate the SIF at the crack front. The proper method to estimate the SIF along the crack front is by a finite element method. Thus, proper consideration of residual stress and its contribution to the propensity for brittle fracture can be accurately determined.

4) The preferred method for determining the SIF is to properly consider all the prevailing loading conditions (residual, operating and internal pressure on crack face), which is the expectation stated in Reference 11, to ensure accurate characterization of the propensity for brittle fracture. Such an effort does result in the SIF exceeding the ASME Section XI allowable.

5) Considering the evaluation for safety factors utilized in the ASME Code, a rational justification for a reduction in the safety factor is proposed. The reduction is justified because it considers the distinction between general membrane and the local membrane stresses.

6) The analysis presented here provides an accurate estimate of SIF and a proper assessment for the potential for brittle fracture. The results

presented here demonstrate that reducing the safety factor continues to maintain sufficient margin against brittle fracture.

References

1) "ANO-1 CRDM Nozzle IDTB J-groove Weld Flaw evaluation"; Framatome ANP Calculation Number 32-5021538-00; Framatome ANP; November 11, 2002. (Framatome Proprietary Document)

2) "Flaw Evaluation Procedures – Background and Application of ASME Section XI, Appendix A"; EPRI Report NP-719-SR; Electric Power Research Institute, Palo Alto, California; August 1978. (EPRI Licensed Material).

3) "Structural Life Assessment Methods"; Alan F. Liu; ASM International; Metals Park, Ohio; 1998.

4) "ANO Unit 1 CRDM Stress Analysis"; Calculation Number C-4154-00-1; Dominion Engineering Inc. Reston, Virginia; November 2002.

5) "PWSCC of Alloy 600 Materials in PWR Primary System Penetrations"; EPRI TR-103696; Electric Power Research Institute, Palo Alto, CA; July 1994.

6) BWR Vessel and Internals Project – Evaluation of crack growth in BWR Stainless Steel RPV Internals (BWRVIP-14)"; EPRI TR-105873; Electric Power Research Institute, Palo Alto, CA; March 1996.

7) "BWR Vessel and Internals Project – Evaluation of crack growth in BWR Nickel Base Austenitic Alloys in RPV Internals (BWRVIP-59)"; EPRI TR-108710; Electric Power Research Institute, Palo Alto, CA; December 1998.

8) ASME Boiler and Pressure Vessel Code, Section XI; 1992 Edition.

9) "CRDM Nozzle ID Temper Bead Weld Repair ANO Unit 1; FTI Drawing number 5021508-03.

10) "Principles of Fracture mechanics"; A. J. Sanford; First Edition; Prentice Hall Limited; 2002.

11) NRC letter, *Request for Additional Information Concerning WCAP-16180NP, Revision 0, "Operability Assessment for Combustion Engineering Plants with Hypothetical Flaw Indications in Pressurizer heater Sleeves" (TAC No. MC1751)* from Mr. D. Holland, Project Manager, Office of NRR, to Mr. G. Bischoff, Manager, owners Group Program Management Office, Westinghouse Electric Company.

12) Calculation No: 86-E-0074-161; "ANO-1 CRDM IDTB Weld Anomaly Flaw evaluations"; Framatome ANP calculation, No: 32-5021539-00; Dated November 5, 2002.

13) "Effect of Residual Stress on Brittle fracture testing"; Michael R. Hill and Tina L. Panontin; *Fatigue and Fracture Mechanics: 29th Volume, ASTM STP 1332;* T. L. Panontin and S. D. Sheppard, Editors; American Society for Testing and Materials; 1998.

Technical Report to Support Relief Request ANO1-R&R-006

14) "Section XI Flaw Acceptance Criteria and Evaluation Using Code Procedures"; Arthur F. Deardorff; Chapter 29, Companion Guide to the ASME Boiler and Pressure Vessel Code, Volume 2; K. R. Rao Editor; ASME Press; 2002.

15) "Subsection NB – Class 1 Components"; John Hechmer; Chapter 6, Companion Guide to the ASME Boiler and Pressure Vessel Code, Volume 1; K. R. Rao Editor; ASME Press; 2002.

Fracture Assessments of Welded Structures

T.L. Panontin, O. Nishioka
NASA Ames Research Center
Moffett Field, CA 94035

Michael R. Hill
University of California
Davis, CA 95616

Summary

Weldments are particularly susceptible to fracture due to defects, material property variations, and residual stresses created during the welding process. It is common in fracture assessments of welded structures to ignore these features; defects are often idealized to be crack-like, weld properties to be homogeneous, and residual stresses to be uniaxial and tensile or nonexistent. This paper presents an overview of several recent studies that examined the ability to accurately model fracture in welds that possess realistic flaws, inhomogeneous material properties, and residual stresses.

Introduction

Welding is a process used to permanently join two, usually metallic, components by the localized coalescence that occurs under certain combinations of temperature, pressure, and metallurgy. The range of pressure and temperature used is quite broad, although heating and cooling are integral parts of most welding processes. The particular combination of these variables results in a unique joint in terms of material variations, potential flaws, and residual stresses.

Material variations occur across a weld joint because each position in the weld is subjected to a different thermal history, with some temperatures rising above those required for phase transformations and grain growth. In a typical multi-pass weld in steel, for instance, several subzones may develop in the heat affected zone (HAZ) between the weld metal and base metal [1], each with its own microstructure and mechanical and fracture properties. Further, if filler metals are used, the weld metal may have significantly different composition than the base metal and hence may possess different mechanical properties. Such variations can cause deformation to be concentrated in the joint, as in the case of weld metals with lower strength than the base plate (undermatched), or to be forced in to the surrounding plate as occurs in overmatched welds [2]. Hence, material variations can affect both the fracture toughness and the concentration of driving force within a joint.

The welding process also largely controls the potential for weld defects to develop during fabrication. For example, the most common defects developed during arc-welding are process-related, and they include lack of penetration (LOP) and lack of fusion (LOF), which are planar or crack-like defects, and slag inclusions and porosity, which are volumetric defects [1]. Cracks may also develop during welding. Planar defects and cracks have direct consequences on the structural integrity of weldments, while volumetric defects may eventually pose problems by initiating fatigue cracks during service.

Residual stresses are created during welding by the solidification, phase transformation, and thermal shrinkage strains associated with molten weld metal as it cools. Existing without external loading, residual stresses are self equilibrating, and often reach magnitudes of yield level. They can cause cracking and distortion in weld joints and even premature failure of structures under certain conditions [1].

These factors, separately and in combination, increase the susceptibility of weldments to fracture. They also greatly complicate the application of fracture assessment methods to welded structures. Prediction of fracture is often performed by assuming that a single, global fracture parameter, such as the J-integral,

completely characterizes the conditions for fracture. However, in welds, the conditions for fracture may be affected by both residual stresses and inhomogeneous materials. Although in the former case superposition can sometimes be used to account for the driving force due to both applied and residual stresses, this requires that existing residual stresses be well characterized. In the case of mismatch where concentration of deformation is dependent on the joint materials, formulas used to estimate J for structural loadings may be inaccurate, particularly when crack sizes are small relative to the thickness of the joint [2]. Single parameter fracture methods also ignore the influence of *constraint* which affects the magnitude of the crack-tip stress fields. Two bodies loaded to the same value of the global fracture parameter, but under differing levels of constraint, will contain different levels of the crack-tip stresses and strains that ultimately set the conditions required for fracture. It has been shown that different levels of constraint can exist in structures due to differences in geometry (e.g., shallow vs. deep notch) or applied loading (e.g, tension vs. bending). Less understood is that constraint changes can also result from the presence of residual stress [3] and weld mismatch [2].

This paper presents an overview of several studies performed to examine the applicability of fracture assessment techniques to weld fracture. In the first study, the fracture behavior of an overmatched butt weld containing a buried, lack-of-penetration defect was predicted and verified experimentally. The second study examined computationally the effect of residual stresses on constraint conditions and subsequent fracture in a cracked weld. In both studies, micromechanical models were used to identify the local conditions at fracture initiation (and subsequent ductile tearing) using crack tip stresses and strains. Finite element analyses were used to predict the influence of specimen/flaw geometry, loading mode, material flow properties, and residual stresses on the crack tip fields. Constraint effects are thus implicitly included; the critical value of the *global* fracture parameter for a particular defective weld is said to be reached when the *local* conditions for fracture are satisfied.

Realistic Flaw Geometries and Weld Material Mismatch

To assess the transferability of R-curves measured in laboratory specimens to defective structural welds, Nishioka and Panontin [4] studied the fracture behavior of an overmatched butt weld containing a simulated, buried lack-of-penetration defect. A specimen designed to simulate pressure vessel butt welds was considered; namely, a center crack panel specimen, of 1.25 in (31.8 mm) by 1.25 in (31.8 mm) cross section, loaded in tension, as shown in Fig. 1a. Specimens were loaded monotonically while load-CMOD measurements were made, then stopped and heat tinted to mark the extent of ductile crack growth. These measurements were compared to predictions made using the fracture mechanics finite element code WARP3D, which implements the Gurson-Tvergaard micromechanical model of void growth to predict ductile tearing.

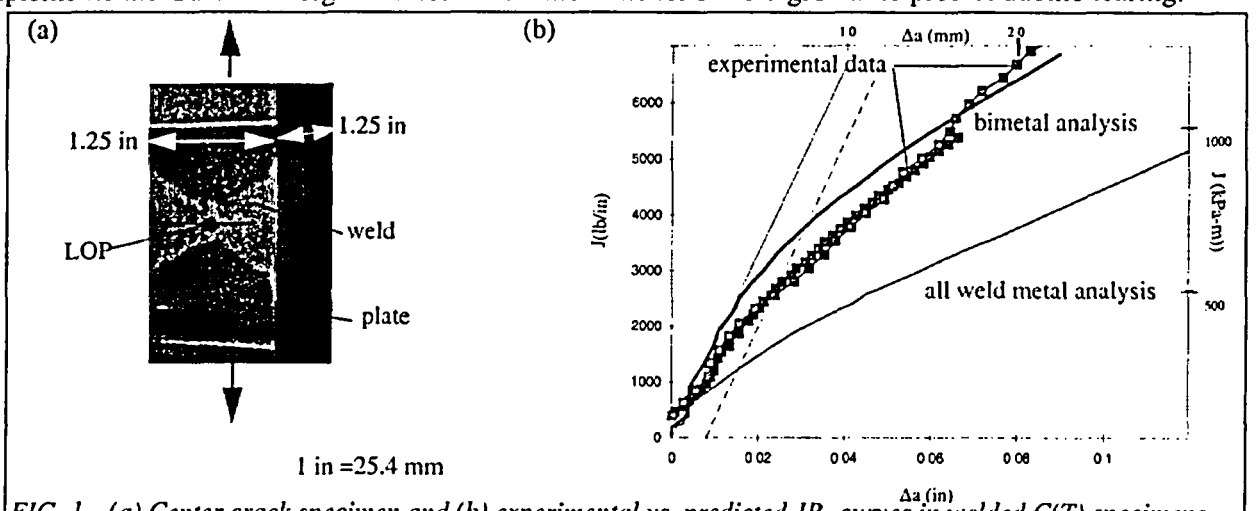

FIG. 1—(a) Center crack specimen and (b) experimental vs. predicted JR- curves in welded C(T) specimens

The stress-relieved, double-V weld tested was comprised of E7018 filler and A516-70 plate, such that the weld had a yield strength 50% higher than that of the plate material. To simulate a lack of penetration defect in the structural weld specimen, a 1/8 inch (3.2 mm) hole was drilled down the center of the weld through which a 0.003 inch (0.076 mm) diameter EDM wire was threaded. The wire was used to introduce crack-like notches toward both surfaces of the weld (Fig. 1a). Welded compact tension specimens were also tested and analyzed to provide model parameters that could not be measured directly. The R-curves measured in compact tension specimens were also compared to those obtained in multi-specimen structural weld tests to examine the issue of transferability of R-curves.

Predictions of *J-R* curves were made using the Gurson-Tvergaard micromechanical model for the process of void growth that culminates in ductile crack growth [5]. A continuum model, it assumes the material acts as a homogenous, porous medium, such that the plastic flow potential is dependent on the hole volume fraction, f. The Gurson-Tvergaard model is implemented within a finite element framework (i.e., WARP3D) by discretizing the material ahead of the crack tip into uniform, fixed-sized cells, with each cell containing an initial void volume fraction, f_o. The cells lie in a single layer along the crack plane of height, D, where D is related to the mean spacing of large inclusions and comparable in size to the measured CTOD at the initiation of ductile tearing [5]. Void growth within the Gurson cells begins immediately upon loading (i.e., void nucleation is neglected). A critical void volume fraction, f_E, is used to assess coalescence. When $f \geq f_E$, the crack tip element is removed (and the crack tip advanced) computationally by reducing the remaining stresses in the element to zero [5].

As suggested by Kirk [2], a "bimetal" model of the weld/plate interface was used, in which the weld and plate are modeled as two distinct materials with no transition or HAZ. The crack front element size was selected from estimates of the weld metal fracture process zone obtained from test and metallographic data. The process zone size, D, was estimated to be about 0.008 inch. In the compact tension, bimetal analyses (with D fixed), f_0 was varied to determine the best fit to the experimental C(T) *J-R* curves, load-CMOD data, and crack front shapes. For D=0.008 inch, it was determined after several iterations that the optimal initial void volume fraction for weld metal is 0.001, as shown in Fig. 1b. For comparison with the bimetal model, an "all weld metal" specimen, in which the entire specimen is modeled as one homogeneous material, was analyzed. As shown in Fig. 1b, *J-R* curve predictions made using the all weld metal model with fracture parameters found from the bimetal analysis diverge significantly from the experimental results. This result clearly illustrates the need to account for material property variations when dealing with welded materials.

Once calibrated with C(T) specimens, the model parameters (D=0.008 in and f_o=0.001) were used in a bimetal finite element analysis to predict the ductile fracture behavior of the more structurally representative CCP specimen geometry. Fig. 2a compares the crack growth profile at a given level of CMOD predicted

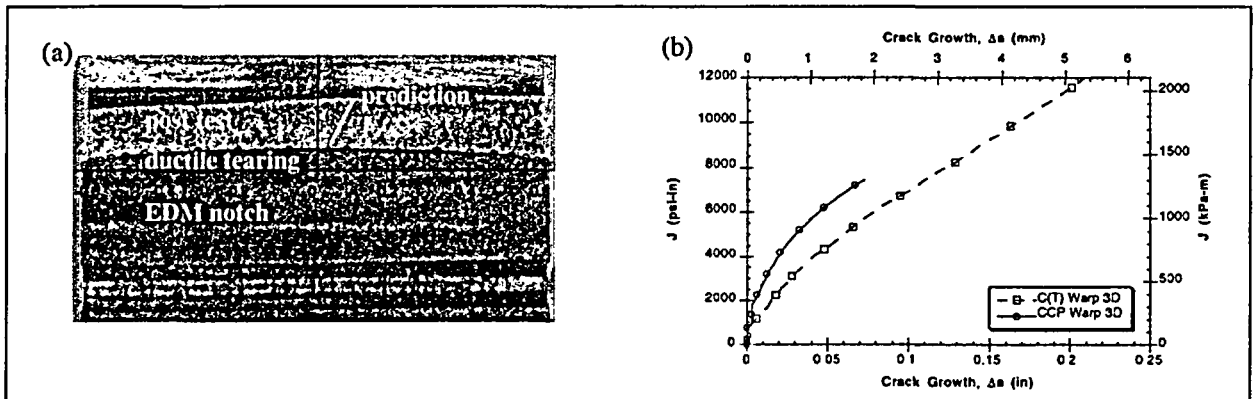

FIG. 2—(a) Fracture surface with overlay of predicted ductile crack growth and (b) predicted J-R curves for compact tensions and center crack specimens. [4]

by the analysis to that obtained experimentally. The predicted amount of crack growth is shown superimposed on the structural specimen fracture surface. The agreement is excellent. Comparison of the (predicted) C(T) and structural (CCP) *J-R* curves in Fig. 2b shows the specimen dependent toughness behavior consistent with previously demonstrated constraint effects [5].

Residual Stresses

The contribution of residual stresses to the driving force for fracture is well known. However, residual stresses may also affect apparent material toughness behavior by changing the constraint conditions under which fracture occurs. To investigate the constraint effects of residual stresses, Panontin and Hill [3] and Hill and Panontin [6] investigated computationally the micromechanics of cleavage fracture in the presence of a realistic residual stress field. The two crack geometries investigated are shown in Fig. 3: a girth-welded pipe representing a "structure" (Fig. 3a) and an SE(B) specimen removed from the structure (Fig. 3b). Homogeneous material properties were assumed to isolate the influence of residual stress on fracture. Material response was assumed to be elastic-plastic and to correspond to normalized A516-70, a high hardening, ferritic, pressure vessel steel with a uniaxial yield strength, σ_o, of 303 MPa (44 ksi).

A three-dimensional residual stress field representative in character of that developed in a two-sided multi-pass weld in a steel plate was considered. The crack plane distributions of residual stress in the pipe are plotted in Fig. 4. The residual stress field of Fig. 4 is generated within the finite element analysis by imposing an eigenstrain field. The label "eigenstrain" refers to the combination of all the non-elastic, incompatible strains set up during the welding cycle [3], which along with the geometry of the structure, completely defines the residual stress state. Here, an idealized eigenstrain distribution was assumed.

The Ritchie, Knott, and Rice, or RKR model for cleavage fracture was used to predict fracture initiation. The RKR model predicts fracture when the opening stress, σ_{yy}, ahead of the crack-tip exceeds a fracture stress, σ_f^*, over a critical distance, l^* [7]. The evolution of opening stress ahead of the crack-tip, due to applied loading alone or in combination with residual stress, was predicted using elastic-plastic, finite strain, finite element analysis. The RKR parameters were assumed to be $\sigma_f^* = 3.5\sigma_o$ and $l^* = 0.15$ mm (0.006 in), about 3 ferritic grain diameters in A516-70 [3].

The change in constraint conditions due to geometry and the influence of the residual stress field were quantified using *J-Q* theory. The theory uses an approximate two-parameter description of the crack-tip stress-strain fields developed from asymptotic analyses and finite element simulations performed by O'Dowd and Shih [8]. As a measure of how much σ_{ij} differs from the adopted small scale yielding (SSY) reference solution at the same applied J, the parameter Q has been shown to characterize the magnitude of the hydrostatic stress over the forward sector ahead of the crack-tip (i.e., $\theta < \pi/2$ and $1 < r/(J/\sigma_o) < 5$ to a good

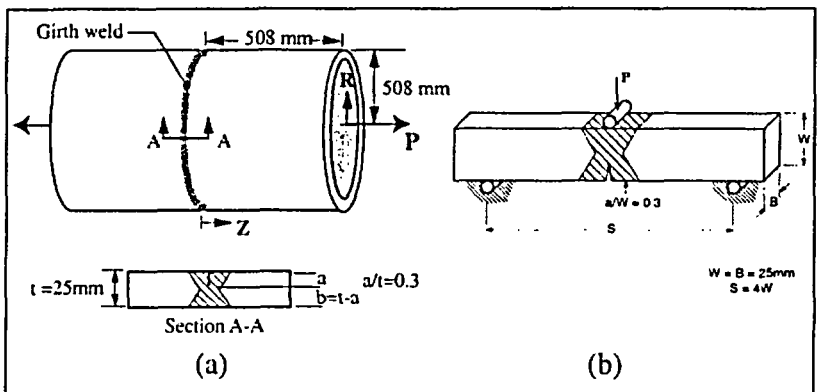

FIG. 3 -(a) pipe and (b) SE(B) specimens considered in residual stress study [9]

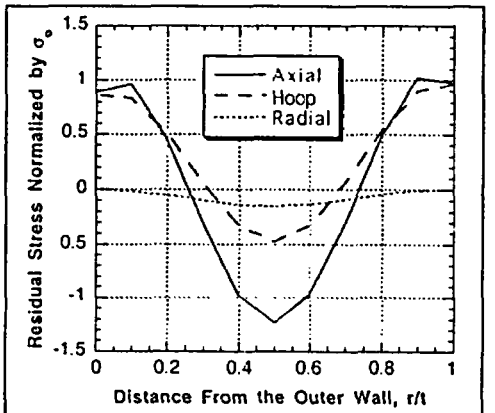

FIG. 4 - residual stress distribution in pipe specimen [9]

approximation. A negative Q-value denotes a loss in constraint, while a positive Q-value indicates that high constraint exists for a particular geometry and loading condition. In this study, Q was determined as

$$Q = [\sigma_{\theta\theta} - \sigma_{\theta\theta}|_{SSY}]/\sigma_o \text{ at } \theta = 0,\ r/(J/\sigma_o) = 4. \qquad (1)$$

Fracture predictions using the superposition and RKR methods are reported in Table 1. At the load corresponding to RKR-predicted fracture, crack-tip opening stresses are nearly the same in each different geometry. As can be seen in Column 2 of Table 1, this occurs at markedly different values of J. For the two non-residual-stress, or "unwelded", cases there is a large difference in RKR-predicted J at fracture, J_c. This demonstrates an anticipated constraint effect since the tension-loaded pipe is significantly less constrained than the SE(B) specimen. Constraint-loss increases crack-tip plasticity, so that additional loading is required to reach a critical crack-tip stress state. For the "welded" cases, the results show that cleavage fracture as predicted by the RKR model is severely affected by the residual stress field; the predicted J-integral for initiation in the pipe decreases by 63% and in the SE(B) geometry by 26%. The difference in the residual stress induced toughness change for each geometry (63% versus 26%) is thought to result from the relative absence of longitudinal welding residual stress in the SE(B) specimen, stresses acting in the hoop direction in the pipe which are released when the SE(B) is cut free.

The effect of geometry and residual stress on crack-tip constraint is also reflected in the J-Q trajectories for each specimen, shown in Fig. 5a. The final point (largest J) on each curve represents the point of predicted fracture initiation. The trajectory developed in the pipe geometry during loading without residual stresses demonstrates the immediate loss of constraint upon loading that is typical of a tension loaded, finite crack geometry. With residual stresses, however, the loss of constraint is delayed until later in the loading history. Near the predicted J-value for cleavage fracture initiation in the welded pipe, the Q-value for the welded pipe is still nearly 0.1 while that for the unwelded pipe is -0.4; this represents a large constraint increase created by the residual stresses. The increased constraint due to residual stress is also clearly mirrored in the plastic zone development at the crack tip, as shown in Fig. 5b. The residual stresses suppress crack tip plasticity and hence increase constraint.

Hill and Panontin [9] examined the accuracy of a superposition prediction of fracture by assuming that the RKR model correctly predicts fracture initiation and that the finite element prediction of J-integral correctly models the superposition of driving forces. A typical assessment would use J_c obtained from standard SE(B) specimen testing with an estimate of driving force to predict fracture (i.e., $J^{Total} = J_c$). The J_c value that would be measured in the unwelded SE(B) specimen in the study is $J_c = 17.0$ kN/m according to the RKR model (Table 1). Using this value of toughness to assess fracture in the unwelded pipe under-predicts the fracture load by 16%, relative to the RKR prediction of 21.3 MN. The prediction is in error because it assumes J-control of crack-tip stresses and ignores constraint-loss in the axially-loaded pipe relative to the SE(B). Using the same approach to predict fracture in the welded pipe, it was found that $J^{Total} = J_c$ at $P_c = 12.2$ MN. This load estimate is *non-conservative* by 24%, relative to the RKR prediction of $P_c = 9.83$ MN, because it ignores both the constraint-loss due to geometry and the constraint-addition caused

Geometry	J_c	*Failure Load, P_c*			
	RKR	*RKR*	*Superposition with RKR J_c from:*		
			SE(B)	*Pipe*	*Welded SE(B)*
SE(B)	17.0 kN/m	35.0 kN	--	--	--
Welded SE(B)	12.6 kN/m	11.7 kN	--	--	--
Pipe	36.7 kN/m	21.3 MN	17.9 MN	--	--
Welded Pipe	13.5 kN/m	9.83 MN	12.2 MN	19.9 MN	9.11 MN

Table 1: J-integral at fracture and fracture load predicted using the RKR and superposition models [9]

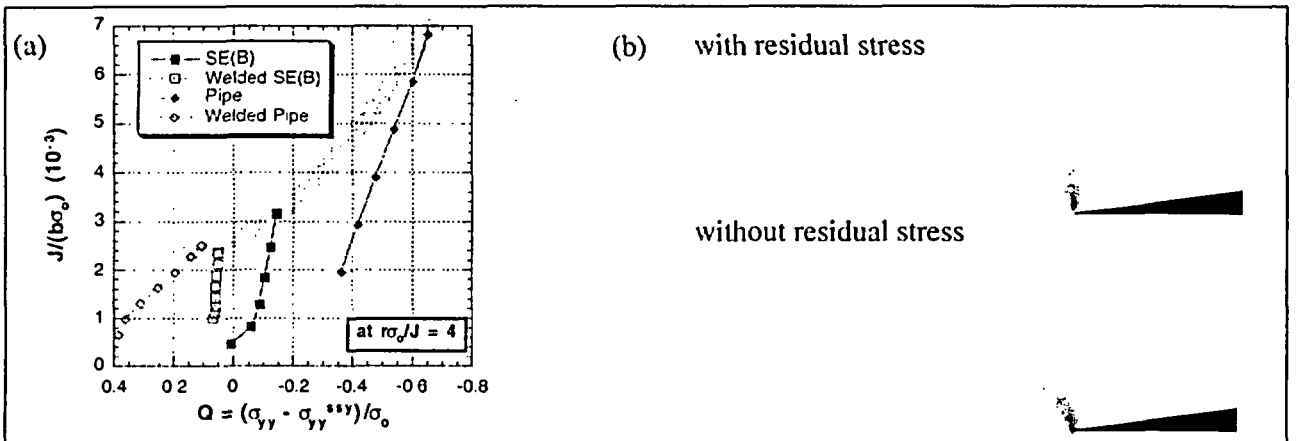

FIG. 5- (a) J-Q trajectories [9] and (b) plastic zone sizes at $J/b\sigma_o$~0.005 [3]

by residual stress. A toughness value might be obtained from the unwelded pipe to account for geometric constraint-loss in the pipe so that J_c = 36.7 kN/m. This leads to a prediction of fracture at P_c = 19.9 MN for the welded pipe, which is *non-conservative by 102%* because it ignores the constraint generated by residual stress.

Conclusions

Several studies were made to investigate the applicability of fracture assessment techniques to welded joints that contain fabrication defects, material property variations, and residual stresses. The results demonstrate the ability to predict ductile crack growth in stress-relieved defective structural welds using the computational cell methodology implemented in WARP3D when weld property differences are considered. Residual stresses are shown computationally to affect both the driving force for fracture and the constraint conditions at the crack tip. Results also show that superposition can account for the driving force but may produce serious errors if the constraint affect is ignored.

References

1. ASM Handbook, Vol. 6., "Welding, Brazing, and Soldering," ASM International, Metals Park, OH.
2. Kirk, M.T., "Predictions of Constraint Effects on Elastic-Plastic Fracture in Welded Structures," Ph.D. Thesis, Univ. of Illinois at Urbana Champaign, (1992).
3. Panontin, T. L. and Hill, M. R. "The Effect of Residual Stresses on Brittle and Ductile Fracture Initiation Predicted by Micromechanical Models," International Journal of Fracture v82 (1996) pp. 317-333.
4. Nishioka, O. and Panontin, T. L., "Ductile Crack Growth from Simulated Defects in Strength Overmatched Butt Welds," Fatigue and Fracture Mechanics: 29th Volume, ASTM STP 1321, West Conshohocken, PA, ASTM (to appear).
5. Ruggieri, C., Panontin, T. L., and Dodds, R. H., Jr. "Numerical Modeling of Ductile Crack Growth in 3-D Using Computational Cell Elements." International Journal of Fracture, v82 (1996) p. 67-95.
6. Hill, M. R. and Panontin, T. L., "Effect of Residual Stress on Brittle Fracture Testing," Fatigue and Fracture Mechanics: 29th Volume, ASTM STP 1321, West Conshohocken, PA, ASTM (to appear).
7. Ritchie, R. O., Server, W. L., and Wullarert, R. A., "Critical Fracture Stress and Fracture Strain Models for the Prediction of Lower and Upper Shelf Toughness in Nuclear Pressure Vessel Steels," Metallurgical Transactions 10A (1979) pp. 1557-1570.
8. O'Dowd, N. P. and Shih, C. F., "Family of Crack-Tip Fields Characterized by a Triaxiality Parameter: Part I-Structure of Fields," Journal of the Mechanics and Physics of Solids v39 (1991) pp. 989-1015.
9. Hill, M. R. and Panontin, T. L., "How Residual Stresses Affect Prediction of Brittle Fracture," in Fatigue, Fracture, and Residual Stresses, PVP series, New York, ASME (to appear),.

ENCLOSURE 4

CNRO-2004-00023

AFFIDAVIT FOR WITHHOLDING INFORMATION FROM PUBLIC DISCLOSURE

AREVA

April 2, 2004
FANP-04-1080

Mr. Guy A. Davant
Entergy Operations, Inc.
P.O. Box 31995
Jackson, MS 39286-1995

Subject: AREVA Document 32-5012424-10, "CRDM Temper Bead Base Weld Analysis"

Reference: Entergy Operations Calculation No. 86-E-0074-154. Rev. 0

Dear Mr. Davant,

Entergy Operation, Inc. requested approval from Framatome ANP, Inc. (FANP) to transmit the subject document under the referenced Entergy Calculation to the NRC. The submittal is based upon a NRC request in support of ANO Relief Request for RV Head CRDM Repairs at ANO-1.

FANP, by this letter approves the submittal of the subject document as noted in the referenced Entergy Calculation in support of the FANP IDTB repair process.

FANP maintains the proprietary status of the document and has enclosed the applicable affidavit for Entergy use.

If there are questions regarding this release, please contact me at (434) 832-3767.

Sincerely,

Stephen G. Son
Project Manager

c: J. Smith, ANO

FRAMATOME ANP, INC.
P.O. Box 10935, 3315 Old Forest Road, Lynchburg, VA 24506-0935
Tel. : (434) 832-3000 - Fax : (434) 832-0622

AFFIDAVIT

COMMONWEALTH OF VIRGINIA)
) ss.
CITY OF LYNCHBURG)

1. My name is James F. Mallay. I am Director, Regulatory Affairs, for Framatome ANP ("FRA-ANP"), and as such I am authorized to execute this Affidavit.

2. I am familiar with the criteria applied by FRA-ANP to determine whether certain FRA-ANP information is proprietary. I am familiar with the policies established by FRA-ANP to ensure the proper application of these criteria.

3. I am familiar with the information contained in two attachments to a letter from Entergy Operations to the NRC (Letter No CNRO-2002-00054). These two attachments are calculation summary sheets (designated 32-5021538 and 32-5021539) that address the flaw evaluation of certain CRDM nozzle welds and are referred to herein as "Documents." Information contained in these Documents has been classified by FRA-ANP as proprietary in accordance with the policies established by FRA-ANP for the control and protection of proprietary and confidential information.

4. These Documents contain information of a proprietary and confidential nature and is of the type customarily held in confidence by FRA-ANP and not made available to the public. Based on my experience, I am aware that other companies regard information of the kind contained in these Documents as proprietary and confidential.

5. These Documents have been made available to the U.S. Nuclear Regulatory Commission in confidence with the request that the information contained in the Documents be withheld from public disclosure.

6. The following criteria are customarily applied by FRA-ANP to determine whether information should be classified as proprietary:

(a) The information reveals details of FRA-ANP's research and development plans and programs or their results.

(b) Use of the information by a competitor would permit the competitor to significantly reduce its expenditures, in time or resources, to design, produce, or market a similar product or service.

(c) The information includes test data or analytical techniques concerning a process, methodology, or component, the application of which results in a competitive advantage for FRA-ANP.

(d) The information reveals certain distinguishing aspects of a process, methodology, or component, the exclusive use of which provides a competitive advantage for FRA-ANP in product optimization or marketability.

(e) The information is vital to a competitive advantage held by FRA-ANP, would be helpful to competitors to FRA-ANP, and would likely cause substantial harm to the competitive position of FRA-ANP.

7. In accordance with FRA-ANP's policies governing the protection and control of information, proprietary information contained in these Documents have been made available, on a limited basis, to others outside FRA-ANP only as required and under suitable agreement providing for nondisclosure and limited use of the information.

8. FRA-ANP policy requires that proprietary information be kept in a secured file or area and distributed on a need-to-know basis.

9. The foregoing statements are true and correct to the best of my knowledge, information, and belief.

SUBSCRIBED before me this 25th day of November, 2002.

Danita R. Kidd
NOTARY PUBLIC, STATE OF VIRGINIA
MY COMMISSION EXPIRES: 12/31/04

ENCLOSURE 5

CNRO-2004-00023

LICENSEE-IDENTIFIED COMMITMENTS

LICENSEE-IDENTIFIED COMMITMENTS

COMMITMENT	TYPE (Check one)		SCHEDULED COMPLETION DATE
	ONE-TIME ACTION	CONTINUING COMPLIANCE	
1. Entergy will provide periodic status information regarding RPV head penetration inspection results throughout the 1R18 inspection period. This may be accomplished via e-mail, telephone conversations, fax, or other means.	✓		During Refueling Outage 1R18